# The barley mutant *multiflorus2.b* reveals quantitative genetic variation for new spikelet architecture

Ravi Koppolu[1‡*], Guojing Jiang[1‡], Sara G Milner[1], Quddoos H Muqaddasi[1,3], Twan Rutten[1], Axel Himmelbach[1], Nils Stein[1,4], Martin Mascher[1,5], Thorsten Schnurbusch[1,2*]

[1]Leibniz Institute of Plant Genetics and Crop Plant Research (IPK), Correns Strasse 3, OT Gatersleben, 06466 Seeland, Germany.

[2]Institute of Agricultural and Nutritional Sciences, Faculty of Natural Sciences III, Martin Luther University Halle-Wittenberg, 06120 Halle, Germany

[3]Current address: BASF Agricultural Solutions GmbH, Am Schwabeplan 8, OT Gatersleben, 06466 Seeland, Germany

[4]Center of integrated Breeding Research (CiBreed), Department of Crop Sciences, Georg-August-University, 37075 Göttingen, Germany

[5]German Centre for Integrative Biodiversity Research (iDiv) Halle-Jena-Leipzig, Leipzig, Germany

[‡]Ravi Koppolu and Guojing Jiang contributed equally

*Corresponding authors:

Ravi Koppolu (koppolu@ipk-gatersleben.de);

Thorsten Schnurbusch (schnurbusch@ipk-gatersleben.de)

ORCIDS

R.K. 0000-0001-8566-9501

G.J. 0000-0002-4335-1527

S.G.M. 0000-0002-1600-5979

Q.H.M. 0000-0001-5961-7273

T.R. 0000-0001-5891-6503

A.H. 0000-0001-7338-0946

N.S. 0000-0003-3011-8731

M.M. 0000-0001-6373-6013

T.S. 0000-0002-5267-0677

**Key message:** Spikelet indeterminacy and supernumerary spikelet phenotypes in barley *multiflorus2.b* mutant show polygenic inheritance. Genetic analysis of *multiflorus2.b* revealed major QTLs for spikelet determinacy and supernumerary spikelet phenotypes on 2H and 6H chromosomes.


## Abstract

Understanding the genetic basis of yield forming factors in small grain cereals is of extreme importance, especially in the wake of stagnation of further yield gains in these crops. One such yield forming factor in these cereals is the number of grain-bearing florets produced per spikelet. Wildtype barley (*Hordeum vulgare* L.) spikelets are determinate structures, the spikelet axis (rachilla) degenerates after producing single floret. In contrast, the rachilla of wheat (*Triticum ssp.*) spikelets, which are indeterminate, elongates to produce up to 12 florets. In our study, we characterized the barley spikelet determinacy mutant *multiflorus2.b* (*mul2.b*) that produced up to three fertile florets on elongated rachillae of lateral spikelets. Apart from the lateral spikelet indeterminacy (LS-IN), we also characterized the supernumerary spikelet phenotype in the central spikelets (CS-SS) of *mul2.b.* Through our phenotypic and genetic analyses, we identified two major QTLs on chromosomes 2H and 6H, and two minor QTLs on 3H for the LS-IN phenotype. For, the CS-SS phenotype we identified one major QTL on 6H, and a minor QTL on 5H chromosomes. Notably, the 6H QTLs for CS-SS and LS-IN phenotypes co-located with each other, potentially indicating that a single genetic factor might regulate both phenotypes. Thus, our in-depth phenotyping combined with genetic analyses revealed the quantitative nature of the LS-IN and CS-SS phenotypes in *mul2.b*, paving the way for cloning the genes underlying these QTLs in the future.



Keywords: spikelet determinacy, supernumerary spikelet, floret formation, rachilla

## Introduction

Grass inflorescences are constituted by the ordered arrangement of spikelets (specialized flower-bearing structures) either directly on the inflorescence axis (rachis) or on the branches differentiated from the inflorescence axis. The Triticeae grasses display characteristic spike-shaped inflorescences with sessile spikelets attached to the inflorescence axis in a distichous phyllotaxis (Bonnett 1935, 1936; Kellogg et al. 2013). Among *Triticeae*, wheat (*Triticum spp.*) and barley (*Hordeum spp.*) represent the most economically important temperate cereal species (Schnurbusch 2019). Based on the architectural differences at the spikelet and spike levels, wheat and barley inflorescences can be classified into (i) determinate or (ii) indeterminate spikes (Bonnett 1966). In the determinate spikes of wheat, the inflorescence apex culminates with a terminal spikelet, producing a fixed number of spikelets per inflorescence. However, the spikelets in the wheat spike are indeterminate with multiple flowers (florets; up to 12), each produced at the articulation junction of the spikelet axis called rachilla (**Fig. 1E)**. In contrast, the inflorescence apex of barley remains indeterminate (no terminal spikelet) and the rachilla ceases to elongate upon initiation of the first floret and remains as a suppressed structure rendering determinacy to the spikelet (**Fig. 1B**). Thus, the spikelet determinacy or indeterminacy is dependent upon the extent of rachilla suppression or elongation.

The genetic control of determinate spikelet fate was studied in rice (*Oryza sativa* L.), wheat, and maize (*Zea mays* L.). In these three species, orthologous APETALA 2 (AP2) transcription factors, such as maize INDETERMINATE SPIKELET1 (IDS1)/TASSELSEED 6 (Chuck et al. 2008; Chuck et al. 2007; Chuck et al. 1998), rice IDS1 (Lee and An 2012), and wheat Q (*AP2L5*) (Debernardi et al. 2017; Greenwood et al. 2017; Simons et al. 2006), were shown to negatively control floret number per spikelet by inhibiting rachilla elongation. The paralog of maize *IDS1*, sister of *IDS1* (*SIDS1*), and rice *SUPERNUMERARY BRACT* also regulate floret number per spikelet by inhibiting rachilla elongation (Chuck et al. 2008; Lee and An 2012; Lee et al. 2007). Interestingly, the corresponding barley ortholog of *IDS1*, i.e., *HvAP2L-H5*, was shown to promote the indeterminate nature of the inflorescence apex and also spikelet determinacy probably by regulating rachilla elongation (Zhong et al. 2021). Apart from the *Q* gene in wheat, the *GRAIN NUMBER INCREASE 1* (*GNI1*) is shown to inhibit rachilla development and growth and thereby regulates floret number per spikelet (Sakuma et al. 2019; Sakuma and Schnurbusch

102 2020). The *sham ramification 1* (*shr1*) and *shr2* mutants in tetraploid wheat show an
103 elongated rachilla. The genes underlying these loci are not known yet (Amagai et al. 2014).
104
105 In rice, genes that potentially regulate spikelet determinacy include *LEAFY HULL STERILE*
106 *1* (*OsMADS1* (Jeon et al. 2000)), *MOSAIC FLORAL ORGANS* 1 (*AGAMOUS LIKE 6* (Ohmori et
107 al. 2009)), and *MULTIFLORETSPIKELET1* (*AP2/ERF*; (Ren et al. 2013)). Mutations in these
108 genes promote rachilla elongation and extra floret formation rendering spikelets
109 indeterminate. Apart from these, rice genes such as *DOUBLE FLORET1/EXTRA GLUME 1*,
110 *FLORAL ORGAN NUMBER 4*, *TONGARI-BOUSHI 1*, and *LATERAL FLORET 1* are also shown
111 to regulate the floret number/spikelet probably through suppression of rachilla
112 elongation (Ren et al. 2019; Ren et al. 2018; Tanaka et al. 2012; Zhang et al. 2017). The
113 results from these studies provided us with a lead that the spikelet determinacy is a plastic
114 trait modulated by the genetic makeup of respective grass species and that the extent of
115 rachilla elongation or suppression potentially defines the floret number per spikelet.
116
117 Within Triticeae, barley shows a distinctive spike architecture, imparted by the
118 distichously arranged triple-spikelet units along the rachis. Each spikelet triplet is
119 constituted by one central (CS) and two lateral spikelets (LS), the two- and six-rowed
120 barley types are defined based on the fertility status at the LSs. In two-rowed barley, the
121 CSs are fertile and produce grains, while LSs remain sterile. Whereas in six-rowed, both
122 CSs and LSs are fertile and bear grains. The fertility status of lateral spikelets is
123 predominantly regulated by the *SIX-ROWED SPIKE 1* (*VRS1,* class I HD-ZIP; (Komatsuda et
124 al. 2007)), along with other regulators/modifier genes (Bull et al. 2017; Koppolu et al.
125 2013; Ramsay et al. 2011; van Esse et al. 2017; Youssef et al. 2017). Thus, the archetypical
126 barley spike possesses one CS positioned on the spike axis with an acute angle, flanked by
127 two LSs positioned slightly away from the spike axis. In wheat, a single spikelet per rachis
128 node is generated with an acute angle to the rachis similar to barley CS. In both wheat and
129 barley, spike mutants that deviate from such a canonical arrangement of spikelets exist
130 that have the potential to generate more spikelets and grains. In barley, a class of mutants
131 called *extrafloret* (*flo*; *flo-a, -b, and -c*) develop either a complete extra or supernumerary
132 spikelet (the locus name *extrafloret* is a misnomer) or rudimentary floral bracts at the
133 base of typical CS on the abaxial side of the same rachis node (Druka et al. 2011; Lundqvist
134 and Franckowiak 2015). The causal genes underlying these loci are not known. A similar
135 supernumerary spikelet (SS) phenotype is also evident in mutants of barley

136 *COMPOSITUM1* (Poursarebani et al. 2020), *COMPOSITUM2* (Poursarebani et al. 2015))
137 and *VRS4* (Koppolu et al. 2013). The wheat ortholog of barley *COM2* was also shown to
138 regulate SS formation in hexaploid (Dobrovolskaya et al. 2015) and tetraploid branched
139 miracle wheat (*TtBH*$^{t}$; (Sakuma and Schnurbusch 2020; Wolde et al. 2019). Apart from
140 these genes, the SS phenotype in wheat is also conditioned by the photoperiod-dependent
141 floral induction gene, *PHOTOPERIOD 1* (*PPD1*), and the axillary meristem growth
142 regulator *TEOSINTE BRANCHED 1* (*TB1*). Both *PPD1* and *TB1* regulate SS formation by
143 regulating *FLOWERING LOCUS T1* (*FT1*) that induces a cascade of floral meristem identity
144 genes important for floral induction (Boden et al. 2015; Dixon et al. 2018).
145
146 In this study, we investigated the inheritance of spikelet determinacy (floret number per
147 spikelet) and supernumerary spikelet phenotypes in a barley *X*-ray induced mutant
148 "*multiflorus2.b*" (*mul2.b;* progenitor–Montcalm). The barley *mul2.b* mutants produce non-
149 canonical multi-floreted, indeterminate spikelets with elongated rachillae, a feature
150 reminiscent of wheat spikelets. Moreover, our in-depth mutant phenotyping and allelism
151 analyses show that *mul2.b* also induces the supernumerary spikelet phenotype. Based on
152 our analyses using exome capture-based bulked-segregant analysis, genetic and QTL
153 mapping studies, we reveal that the multi-floreted and supernumerary spikelet
154 phenotypes show quantitative inheritance patterns.
155
156 **Materials and Methods**
157 ***Plant material and growth conditions***
158 All experiments reported in this study were conducted at the Leibniz Institute of Plant
159 Genetics and Crop Plant Research, Gatersleben, Germany. Barley genotypes cv. Montcalm,
160 cv. Morex, *multiflorus2.b* (*mul2.b;* GSHO 1394) – a betatron induced *X*-ray mutant of
161 Montcalm, and Bowman Near Isogenic line mutant *extra floret.a* – BM-NIL(*flo.a*), were
162 used for various analyses conducted in this study. The majority of experiments were
163 conducted under greenhouse conditions at the IPK in the period between 2014 and 2020.
164 For greenhouse experiments, initially, barley grains were germinated in 96 well planting
165 trays and grown at 16h/8h (light/dark; photoperiod), and, 20°C/16°C (light/dark;
166 temperature) for two weeks. After collecting leaf material for DNA extraction, the plants
167 were vernalized at 4°C for four weeks and then acclimatized at 15°C in the greenhouse
168 for a week. Later the plants were potted into 14 cm (Ø) pots and grown at 16h/8h
169 (light/dark; photoperiod), and, 20°C/16°C (light/dark; temperature) until maturity.

170 Standard practices for irrigation, fertilization, and control of pests and diseases were
171 followed. The genotypes Montcalm and *mul2.b* were evaluated under field conditions in
172 2015 and 2016 at IPK for the grain morphometry parameters. Each genotype was grown
173 in three independent plots measuring 1 × 1.5 $m^2$, with a sowing density of 300 grains/$m^2$.
174 Each plot consisted of six rows with 20 cm spacing between rows.
175
176 ***Mapping populations and phenotyping***
177 For genetic mapping of the traits lateral spikelet indeterminacy (LS-IN) and central
178 spikelet supernumerary spikelet (CS-SS) phenotypes, the mutant parent *mul2.b* was
179 crossed with Morex and Montcalm to generate two independent mapping populations,
180 Morex × *mul2.b* and *mul2.b* × Montcalm. The $F_1$ hybrids were selfed and the resulting $F_2$
181 individuals and $F_{2:3}$ families were used for phenotypic and genotypic analyses. To test the
182 allelism between *mul2.b* and BM-NIL(*flo.a*), reciprocal crosses were made between the
183 two mutants, and the CS-SS phenotype were analyzed at $F_1$ and $F_2$ generations.

184 The Morex × *mul2.b* (POP 2014-1; 163 $F_{2s}$) and *mul2.b* × Montcalm (POP 2014-2; 130 $F_{2s}$)
185 populations were initially phenotyped in 2014 under greenhouse conditions. The LS-IN
186 phenotype was scored as strong or moderate to weak and wildtype based on visual
187 observation of rachilla elongation or extra floret phenotype in all spikes of each $F_2$ plant
188 after grain filling. $F_2$ plants with strong phenotype showed approximately 75% of spikes
189 with a second floret that either produced a grain or remained empty. Whereas the $F_2$ lines
190 that showed elongated rachilla or improperly formed second floret were scored into weak
191 to moderate phenotype class. The CS-SS phenotype in central spikelets was quantified by
192 counting the number of occurrences of extra spikelets or rudimentary bract-like
193 structures on all spikes of each $F_2$ plant.

194 In 2015, we phenotyped Morex × *mul2.b* population again under greenhouse conditions
195 (136 $F_{2s}$; POP 2015) by quantifying both LS-IN and CS-SS phenotypes. For quantification,
196 of LS-IN phenotype we classified the phenotype into *mul2.b* class-*I, -II, -III,* and -*IV* based
197 on the additional floret or rachilla elongation phenotype (please see results section for
198 the description of each phenotypic class). The number of instances of *mul2.b-I, -II, -III,* and
199 -*IV* phenotypes were recorded for all lateral spikelet positions on spike-bearing tillers of
200 each $F_2$ plant. Similarly, the number of instances of supernumerary spikelets born from
201 the central spikelet region was counted.

202 In 2016, a relatively larger $F_2$ population of Morex × *mul2.b* was further phenotyped under
203 greenhouse conditions (179 $F_{2s}$; POP 2016) for the LS-IN and CS-SS phenotypes. The
204 phenotype quantification data from POP 2016 was used for whole-genome QTL mapping.

205 For scoring the CS-SS trait in $F_{2s}$ of BM-NIL(*flo.a*) × *mul2.b*, the phenotype was classified
206 into six classes. These include WT (no phenotype), very weak (one spike with CS-SS
207 phenotype out of all spikes/plant), weak (~10-15% of spikes with CS-SS phenotype),
208 moderate (~25% of spikes with CS-SS phenotype), strong (~50% of spikes with CS-SS
209 phenotype), and very strong (~75-100% of spikes with CS-SS phenotype.)
210

211 ***Grain morphometry analysis of Montcalm and mul2.b***

212 To evaluate grain morphometry parameters of Montcalm and *mul2.b*, spikes from the field
213 (2015 and 2016) and greenhouse (2020) grown plants were hand-harvested and
214 threshed. Representative grain samples from each genotype (3–4 grain
215 samples/plot/genotype) were analyzed for the thousand-grain weight (TGW), grain area
216 ($mm^2$), grain width (mm), and grain length (mm) using a digital seed analyzer/counter
217 Marvin (GTA Sensorik GmbH, Neubrandenburg, Germany). From the greenhouse
218 experiment (2020), the grain morphometry parameters were collected for central and
219 lateral spikelet grains independently. For this analysis, central and lateral spikelet grains
220 of twelve independent plants from each genotype were used. Apart from these, traits such
221 as plant height, total productive and unproductive tillers were scored from the
222 greenhouse experiment (2020).
223

224 ***Phenotyping of Montcalm and mul2.b immature spikes***

225 Immature spikes of Montcalm and *mul2.b* genotypes were phenotyped from Waddington
226 stage W2.0 (double ridge) to W6.0 (Waddington et al. 1983) to follow rachilla
227 development in lateral spikelets. The spike meristems from respective genotypes were
228 hand dissected and staged under a stereomicroscope (Zeiss Stemi 2000-C; Carl Zeiss™).
229 The maximum yield potential in Montcalm and *mul2.b* (number of rachis nodes per spike
230 * three spikelets per node) was counted on the main culm spike approximately at W8.0.
231

232 ***Scanning electron microscopy***

233 Scanning electron microscopy (SEM) was performed on immature spikes that are
234 approximately at W4.0, W4.5, W5.0, W5.5, and W6.0 (central spikelet staging) from

235 greenhouse-grown plants. SEM was conducted following an established protocol at IPK
236 (Lolas et al. 2010; Poursarebani et al. 2020).
237
238 ***Exome sequencing of Morex × mul2.b – POP 2014-1***
239 For exome sequencing, the DNAs from 25 wild type and 27 mutant $F_2$ lines were bulked
240 from Morex × *mul2.b* population grown in 2014. The two DNA bulks were subjected to
241 exome capture and sequencing according to Mascher et al. (2013). Read mapping, allele
242 frequency visualization, and read depth analysis of exome sequencing data of mutant and
243 wild-type bulks were performed as described in Mascher et al. (2014) using the POPSEQ
244 map.
245
246 ***Marker development, linkage, and QTL analysis on 2H and 6H chromosomes***
247 The LS-IN and CS-SS phenotype data from Morex × *mul2.b*–2015 (POP 2015) was used for
248 marker and phenotype linkage analysis on 2H and 6H barley chromosomes. For mapping,
249 the polymorphic SNPs were selected based on exome capture SNPs from chromosomes
250 2H and 6H where allele frequency differences between mutant and wild type bulks
251 reached their maximum. On chromosome 2H, 11 SNPs were selected in the interval 33.70–
252 87.70 cM (Morex POPSEQ positions). On 6H, seven SNPs were selected in the interval
253 31.90–92.20 cM. Selected SNPs were converted to restriction enzyme-based Cleaved
254 Amplified Polymorphic Sequence (CAPS) markers (**Supplementary Table 1**) using Neb
255 cutter v2.0 (New England Biolabs Inc). Restriction digestion was performed according to
256 the manufacturer's protocols. Resulting DNA fragments were separated on 2% agarose
257 gels for genotyping. Genotypic and phenotypic data were subjected to linkage and QTL
258 analyses in Joinmap 4.1 and Genstat 19 respectively.
259
260 ***GBS library construction, sequencing, read alignment, and variant calling***
261 Total genomic DNA from the $F_2$ lines of Morex × *mul2.b* (POP 2016) was extracted as
262 described in Poursarebani et al. (2020). Genomic DNA was digested with *PstI* and *MspI*
263 restriction enzymes and processed for GBS library construction as described in Wendler
264 et al. (2014). Individually barcoded samples were pooled in equimolar concentrations and
265 sequenced on the Illumina HiSeq 2500 (single-read, 107 cycles), using custom sequencing
266 primer (Wendler et al. 2014) as given in manufacturers protocol (Illumina Inc).

GBS reads were trimmed using cutadapt (Martin 2011) and aligned to the reference genome sequence of Morex (Mascher et al. 2017) with BWA-MEM v0.7.12a (Li 2013). Alignment files were converted to binary alignment map (BAM) format with SAMtools (Li et al. 2009), sorted by reference position, and indexed with NovoSort (Novocraft Technologies Sdn Bhd, Malaysia, http://www.novocraft.com/). Variants were called using SAMtools/BCFtools v1.3 specifying the option '-DV' while running SAMtools mpileup (Li 2011) ), to obtain the per-sample number of non-reference reads. An AWK script (available at https://bitbucket.org/ipk_dg_public/vcf_filtering) was used to filter the Variant Call Format (VCF) output file and call genotypes based on the ratio between the depth of the alternative allele and the total read depth (DV /DP). A minimum mapping quality score of 40 was applied. The SNP matrix was created applying the following threshold: a minimum read depth of 2X per genotype and an overall maximum fraction of missing calls of 80%. Only biallelic SNPs were considered. Data for SNPs was filtered with ≤10% missing data points, two or more linked markers showing identical marker scores across all $F_2$ individuals (no recombination), and variants showing distorted marker scores. The final variant set was composed of 605 markers and was used for genetic linkage mapping.

***Whole-genome linkage mapping with GBS markers***

Genetic linkage maps were constructed with data from 605 GBS markers. Markers were initially grouped according to the SNP physical position assignment based on Morex reference. Markers from each group were then ordered using the maximum likelihood mapping algorithm and default linkage parameters in Joinmap 4.1. Recombination frequencies between markers were converted to map distances by the Kosambi mapping function.

***Phenotypic data analyses of Morex × mul2.b–POP 2016***

Phenotypic data for LS-IN and CS-SS traits were collected from up to 12 tillers. To calculate the individual variance components of the genotype, tillers, and residuals, the following linear mixed-effect model was used by assuming all effects except the intercept as random:

$$y_{ij} = \mu + g_i + t_j + \varepsilon_{ij} \quad (1)$$

where, $y_{ij}$ is the phenotypic value of the $i^{th}$ genotype in the $j^{th}$ tiller, $\mu$ is the common intercept term, $g_i$ is the effect of the $i^{th}$ genotype, $t_j$ is the effect of the $j^{th}$ tiller, and $\varepsilon_{ij}$ is

299 the corresponding residual term as $\varepsilon \sim N(0, I\sigma_\varepsilon^2)$ with $I$ and $\sigma_\varepsilon^2$ being the identity matrix
300 and residual variance, respectively. The repeatability ($H^2$) among the tillers was
301 accordingly calculated as:

302 $$H^2 = \frac{\sigma_g^2}{\sigma_g^2 + \left(\frac{\sigma_{\sigma_\varepsilon^2}^2}{nT}\right)} \quad (2)$$

303 where, σ_g^2 and σ_ε^2 denote the variance components of the genotype and residuals,
304 respectively; nT represent the number of tillers. The best linear unbiased estimations
305 (BLUEs) across tillers for a given genotype were calculated by assuming the intercept and
306 genotype effects as fixed in eq. 1. It should be noted that we evaluated the traits in an $F_2$
307 population; therefore, by necessity, we collected the phenotypic data from single plants.
308 The calculations mentioned above were performed to (i) observe if there exists a large
309 and significant (P<0.001) variance for the spike bearing tillers, and (ii) normalize the
310 phenotypic value of the investigated traits per spike since it gives a more meaningful view
311 of the studied traits. The BLUEs were plotted in the form of histograms. To observe the
312 genetic nature of the investigated traits, the Shapiro-Wilk test was performed to monitor
313 if the data were normally distributed at P<0.05. Moreover, to observe the genetic
314 relationship among the investigated traits, Pearson's product-moment correlation was
315 calculated based on the BLUEs as:

316 $$r = \frac{\sum_{i=1}^{n}(x_i - \bar{x})(y_i - \bar{y})}{\sqrt{\sum_{i=1}^{n}(x_i - \bar{x})^2}\sqrt{\sum_{i=1}^{n}(y_i - \bar{y})^2}} \quad (3)$$

317

318 where $x$ and $y$ denote the BLUEs of the studied traits. Unless stated otherwise, all
319 calculations were performed in software R (R core team) using package lme4 (Bates et al.
320 2015).

321 ***Whole-genome QTL mapping in Morex × mul2.b–POP 2016***

322 The BLUEs from LS-IN (*mul2.b-I, -II, III*, and *-IV*) and CS-SS phenotypes and 605 GBS
323 marker data were used for QTL mapping in Genstat 19. Initially, simple interval mapping
324 (SIM) was conducted with single environment, single trait linkage analysis. A step size of
325 5 cM, genome-wide significance level (alpha) of 0.05, and minimum co-factor proximity
326 of 50 cM were used for QTL detection. The minimum separation distance for two
327 consecutive QTLs was set at 30 cM. The co-factors identified from SIM were used for QTL

328 analysis by composite interval mapping (CIM). This process was repeated until no new
329 QTLs were detected. The final QTL model was selected based on background selection
330 (significance 0.05) on the selected co-factors. QTL boundaries (lower and upper),
331 additive, dominance effects, and phenotypic variation explained by the QTL were defined
332 by using the final QTL model. The procedure was repeated for QTL detection in all traits
333 scored. Genetic linkage maps and QTL data were graphically represented using MapChart
334 2.2 (Voorrips 2002).

335 ***Phenotypic analysis of LS-IN and CS-SS in $F_{2:3}$***

336 To validate the genetic and phenotypic effects among QTL loci identified in $F_2$, we
337 performed the phenotypic analysis in $F_{2:3}$ for LS-IN and CS-SS phenotypes. For this
338 purpose, we have generated an $F_{2:3}$ population comprising 1180 individuals segregating
339 for Morex and *mul2.b* alleles at 2H and 6H QTLs. The $F_{2:3}$ lines were genotyped with at
340 least four CAPS markers linked to the 2H (M269389, M5729, 2560790, and M49460) and
341 two markers linked to 6H (FL277086, and FL42060) QTLs. All $F_{2:3}$ lines were phenotyped
342 for floret number in LSs and SS phenotype in CSs. The combinations of 2H and 6H allele
343 frequencies and the corresponding phenotypic values for the respective genotypes are
344 plotted as box plots. All box plots in this study were generated using BoxPlotR (Spitzer et
345 al. 2014).

346 **Results**

347 ***Lateral spikelet determinacy is relaxed in the multiflorus2.b***

348 Spikelets of barley are commonly determinate structures with a single floret being
349 produced per spikelet on its axis i.e. rachilla. After the first floret formation, the elongation
350 of the rachilla is stopped and the rest of the rachilla remains as a thin, pale yellow colored
351 suppressed structure adaxial to the floret (positioned between rachis and palea of the
352 floret; **Fig. 1A, B**). This scenario applies to both CS and LSs of all spikelet triplets along the
353 inflorescence axis. However, in the LSs of *mul2.b* mutants, upon initiation of the first floret
354 (LS-F1), the rachilla further elongates which leads to the development of a second floret
355 (LS-F2) at the articulation junction of the elongated rachilla (**Fig. 1A, C**). In *mul2.b*
356 mutants, the elongated rachilla becomes visible on the adaxial side of the second floret
357 (LS-F2; **Fig. 1C**). Often the elongated rachilla on the second floret of *mul2.b* LSs is enlarged,
358 pale green-colored, indicating that the rachilla elongation is not completely abolished
359 after the second floret formation. In line with this, the rachilla in *mul2.b* LS occasionally
360 elongates beyond the second floret and bears a third floret (LS-F3; **Fig. 1D**). Thus, the

361 rachilla elongation suppression in LSs appears to be lost in *mul2.b* rendering the lateral
362 spikelets indeterminate, a feature reminiscent of indeterminate wheat spikelets (**Fig. 1E**).
363 The rachilla elongation and formation of second and third florets were predominantly
364 restricted to the basal half of the spike (**Fig. 1A**)
365
366 To understand the developmental events during the rachilla primordium initiation and
367 elongation, we undertook scanning electronic microscopy (SEM) analysis initially in wild-
368 type progenitor Montcalm. The general barley spike meristem developmental
369 progression starts with the transition of vegetative shoot apical meristem into
370 reproductive inflorescence meristem (IM). The IM initiates spikelet ridge meristem that
371 further differentiates into one central (CSM) and two lateral spikelet meristems (LSM),
372 followed by the formation of two glume primordia in the flanks of each spikelet meristem
373 (Koppolu and Schnurbusch 2019). At this point, in Montcalm we observed that the floret
374 meristem (FM) first differentiates lemma primordium on the abaxial side. After the
375 initiation of lemma primordium, the adaxial side of the floral meristem buds-off to initiate
376 the rachilla primordium (**Fig. 2A**). Later the residual floral meristem is consumed into the
377 initiation of lodicule, stamen, and carpel primordia (**Fig. 2B-E**). The turn of meristem
378 differentiation events is identical in both CSM and LSM. However, visualizing rachilla
379 primordium in CSM is technically challenging especially at the very early stages of spike
380 meristem development due to the acute angle between CSM and the axis of the spike
381 meristem. Hence, we followed the rachilla primordium development in LSs that are
382 positioned away from the spike meristem axis at appropriate floral primordia initiation
383 time points. In general, the organ primordia differentiated from the floret meristem of
384 Montcalm tended to grow normally with an apparent increase in size over the immature
385 spike developmental phases analyzed (**Fig. 2A-E**). However, the rate of rachilla
386 primordium growth appeared to be slowed down compared to other organ primordia
387 differentiated from the FM (**Fig. 2A-E**). At around W5.0 (central spikelet staging), the
388 rachilla is barely visible in the lateral spikelets at the base and middle of the spike (the
389 developmentally advanced portion of the spike; **Fig. 2C**). Later on, during the spike
390 growth period, the rachilla ceases to grow and remains as a suppressed structure in
391 Montcalm (as seen in **Fig. 1A, B**). In the *mul2.b* mutant, the rachilla primordium was
392 initiated after the differentiation of lemma primordium similar to Montcalm (**Fig. 2F**).
393 Nevertheless, the rachilla primordium of *mul2.b* LSs was not retarded in development and
394 continued to increase in size along with other floral organs differentiated from floret

395 meristem (**Fig. 2F-K**). Over different phases of immature spike development, the rachilla
396 primordium elongated further to form a second FM (**Fig. 2I**). Importantly, the rachilla
397 elongation and formation of additional FM in *mul2.b* was restricted to the LSs; whereas,
398 the rachilla of CS remained as a suppressed structure (**Fig. 2K**).
399
400 Since the LSs of *mul2.b* mutants produced additional florets that are frequently fertile and
401 grain-bearing, we evaluated various yield and biomass-related traits in *mul2.b* and
402 Montcalm. Interestingly, the immature spikes of *mul2.b* showed a significantly increased
403 maximum yield potential compared to Montcalm (Median spikelet number at W8.0–
404 Montcalm 88.5 spikelet primordia; *mul2.b* 102 spikelet primordia; p-value: 5.07E-13).
405 However, the number of fertile spikelets was significantly lowered in *mul2.b* (Median
406 fertile spikelets – 39 in *mul2.b*, 45 in Montcalm; p-value: 0.001) probably owing to the
407 enhanced sink strength in the basal half of the spike and consequent post-anthesis growth
408 abortion of spikelets in the apical part of the spike (**Fig. S1A-C**). The grain parameters
409 such as thousand-grain weight (TGW), grain area (GrA), width (GW) and length (GL) did
410 not show significant differences between Montcalm and *mul2.b* when grains from CS and
411 LS were analyzed together (**Fig. S2A-D**). However, the differences for these traits became
412 apparent between Montcalm and *mul2.b* when the CS and LS grains were measured
413 separately. Interestingly the TGW of CS grains was significantly increased in *mul2.b* (p-
414 value: 0.020) due to the slight increase in grain area, mainly contributed by the increase
415 in GW (**Fig. S2E-H**). The TGW of LSs did not show a significant difference between
416 Montcalm and *mul2.b* (**Fig. S2I**). The parameters GW and GL followed opposite tendencies
417 in *mul2.b* LSs where GW was slightly higher and GL was significantly lowered (p-value:
418 3.61E-05) compared to Montcalm, probably leading to similar GrA and TGW (**Fig. S2I-L**).
419 Apart from the grain parameters, the plant height was significantly reduced in *mul2.b* (p-
420 value: 0.020), whereas the number of tillers including productive spike-bearing tillers and
421 unproductive tillers remained the same (**fig. S1D-G**).
422
423 ***Lateral spikelets of mul2.b display a gradual rachilla elongation phenotype***
424 The extent of rachilla elongation and the type of additional structures being formed in the
425 LSs of *mul2.b* varied among spikelets of each spike. To quantify these additional
426 structures, we devised a score to classify them into four phenotype component classes
427 such as *mul2 – class I* (*mul2-I*), *mul2-II*, *mul2-III*, and *mul2-IV*. The *mul2-I* had the strongest
428 LS rachilla elongation phenotype with the formation of a second floret that is often fertile

429 and an occasional third floret (**Fig. 3B, C,** and **Fig. S3B**). Also, the second floret with an
430 elongated awn is part of the *mul2-I* class. The reproductive organ development is mostly
431 complete in *mul2-I* except for the occasional lack of carpel growth. The second floret of
432 *mul2-II* is comparatively smaller without awn elongation (**Fig. 3D, E** and **Fig. S3C**).
433 Occasionally, the second floret in the *mul2-II* class had stamens but carpel growth is
434 completely abolished. In the *mul2-III* class, the unsuppressed rachilla showed bi- or
435 trifurcation at the base that further elongated into filament-like structure (**Fig. 3F, G** and
436 **Fig. S3D**). The *mul2-IV* phenotypic class is similar to *mul2-III* except that the
437 unsuppressed rachilla did not elongate into a filament-like structure (**Fig. 3H, I** and **Fig.**
438 **S3E**). In both *mul2-III*, and *-IV* the elongated rachilla did not attain a second floret identity
439 as seen in *mul2-I* and *mul2–II*. The spatial occurrence of *mul2-I, -II, -III, -IV* individual
440 component classes did not show any preferential pattern in the spike indicating the
441 random nature of their occurrence along the spike axis (**Fig. S4**). Throughout this report,
442 we referred to the rachilla elongation phenotype of LSs as lateral spikelet indeterminacy
443 (LS-IN).
444
445 ***Supernumerary spikelet formation in central spikelets of mul2.b***
446 In contrast to the loss of spikelet determinacy in the LSs, the *mul2.b* mutant showed
447 another interesting feature: the formation of supernumerary spikelets (SS) exclusively in
448 the CS. The SSs were formed abaxial to the typical CSs (**Fig. 1F**). The observed
449 supernumerary spikelet phenotype in *mul2.b* ranged from the formation of rudimentary
450 floral bract-like structures to complete spikelets with occasional grain formation (**Fig.**
451 **1F**). Such a SS phenotype is also evident in the barley mutant *extrafloret.a* (BM-NIL(*flo.a*).
452 Interestingly, the SSs that originated at the CSs were occasionally indeterminate with
453 rachilla elongation and formation of second floret similar to the indeterminate LS
454 phenotype in *mul2.b* (**Fig. 1F**). In this report, we termed the SS phenotype on the CS as
455 "CS-SS".
456
457 ***Genetic mapping identifies genomic regions responsible for the LS-IN and CS-SS***
458 ***phenotypes***
459 Previous studies reported that the LS-IN trait in *mul2.b* showed a monogenic recessive
460 inheritance pattern (Walker et al. 1963). Hence, we developed two $F_2$ mapping
461 populations by crossing *mul2.b* with Morex (Morex × *mul2.b*; POP 2014-1) and Montcalm
462 (*mul2.b* × Montcalm; POP 2014-2) for genetic mapping. Of the 163 $F_2$ lines phenotyped

463 from POP 2014-1, 35 and 83 $F_{2s}$ showed strong and weak to moderate LS-IN phenotypes,
464 respectively, while 45 $F_{2s}$ were WT, suggesting that the observed phenotype segregation
465 was in contradiction with the previously proposed monogenic recessive inheritance
466 pattern for the LS-IN trait (Walker et al. 1963). From our phenotypic analysis, the LS-IN
467 phenotype appeared to follow an incomplete dominance with homozygous mutant $F_{2s}$
468 showing strong and the heterozygous $F_{2s}$ showing weak to moderate LS-IN phenotypes
469 ($\chi 2$ = 0.591, *p-value* = 0.442). A similar incomplete dominant inheritance was also
470 observed for the POP 2014-2 (**Supplementary Table 2**). With respect to the CS-SS
471 phenotype, 99 $F_{2s}$ of POP 2014-1 showed the phenotype whereas 64 $F_{2s}$ did not show a
472 phenotype; and hence, were wild type for CS-SS. The majority of the $F_{2s}$ with CS-SS
473 phenotype also had the LS-IN phenotype (70 out of 99 $F_{2s}$), while 29 $F_{2s}$ that were wild
474 type for LS-IN also showed a weak CS-SS phenotype. Thus, the phenotypic inheritance
475 analysis in $F_{2s}$ indicated that the *mul2.b* phenotype is in fact a combination of LS-IN and
476 CS-SS phenotypes.
477
478 For identifying the genomic region(s) harboring the *mul2.b* mutation, we adopted
479 sequencing-based bulked-segregant analysis (BSA) by exome capture (Mascher et al.
480 2014; Mascher et al. 2013). To this end, DNAs from 27 mutant $F_{2s}$ with a strong LS-IN
481 phenotype, of which 20 individuals also had the CS-SS phenotype (**Figure 4A**), and 25
482 wild-type $F_{2s}$ were pooled to form the LS-IN/CS-SS mutant and wild-type bulks. The two
483 bulks were subjected to exome capture and subsequently sequenced on Illumina
484 Hiseq2000. The single nucleotide polymorphisms were identified by mapping sequence
485 reads onto the Morex reference genome. The SNP allele frequencies from the two pools
486 were visualized along the barley physical and genetic maps. Surprisingly, the allele
487 frequency distribution showed two distinct peaks on chromosomes 2H and 6H where in
488 both cases the mutant allele frequencies for the combined LS-IN/CS-SS phenotype
489 increased over 75% and wt allele frequency dropped to about 25% (**Fig. 4B**).
490
491 ***A novel locus regulates the CS-SS phenotype in mul2.b***
492 In our BSA, allele frequencies peaked on 2H and 6H, indicating that the combined
493 phenotypes of LS-IN and CS-SS are regulated by two independent loci in *mul2.b*. Previous
494 genetic analyses linked the *flo.a* phenotype on the short arm of 6H (Druka et al. 2011).
495 Interestingly, the CSs of the barley BM-NIL(*flo.a*) mutant showed the identical CS-SS
496 spikelet phenotype (Lundqvist and Franckowiak 2015) as *mul2.b* (**Fig. 5A-B**), providing

497 the possibility that both loci might be identical. To examine this idea (**Fig. 5A-B**), we made
498 reciprocal crosses between these two mutant loci to evaluate allelism between them. The
499 CS-SS phenotype in *flo.a* was previously shown to follow a monogenic recessive
500 inheritance (Gustafson 1969). The $F_{1s}$ generated from the *mul2.b* and BM-NIL(*flo.a*)
501 crosses showed a strong CS-SS phenotype (**Fig. 5A-C**), potentially suggesting that the CS-
502 SS phenotype in both BM-NIL(*flo.a*) and *mul2.b* is regulated by a single locus. However,
503 evidence can only be provided by checking phenotypes of $F_{2s}$. We therefore evaluated the
504 $F_2$ generation of the BM-NIL(*flo.a*) × *mul2.b* cross for the CS-SS phenotype to further verify
505 the potential allelic relation of *flo.*a and *mul2.b*. Surprisingly, we found segregation for the
506 CS-SS phenotype among the $F_2$ progenies: i.e. of the 395 $F_{2s}$ analyzed, 106 did not show
507 the CS-SS phenotype, whereas 289 $F_{2s}$ showed a very weak to very strong CS-SS
508 phenotype (**Fig. 5D**). The observed phenotype segregation in $F_2$ thus indicated that the
509 CS-SS phenotype in *mul2.b* and *flo.a* is most likely regulated by two-independent loci (**Fig.
510 5E**). The allele and phenotype proportion analysis for the BM-NIL(*flo.a*) × *mul2.b* dihybrid
511 cross showed that the 6H locus regulating the CS-SS phenotype in *mul2.b* followed a
512 recessive inheritance ($\chi 2$ = 3.859, *p-value* = 0.0495). From our exome capture data, the
513 highest allele frequency difference for the 6H peak lied between 59.92 – 61.05 cM
514 (POPSEQ position), whereas the *flo.a* locus was mapped to 52.20 cM (data not shown),
515 indicating that the CS-SS phenotypes in *mul2.b* and *flo.a* are regulated by two independent
516 loci on 6H.
517
518 ***Genetic linkage of the LS-IN and CS-SS phenotypes to 2H and 6H***
519 To conduct a rough genetic linkage analysis of the LS-IN and CS-SS phenotypes we
520 selected 11 SNPs on 2H (33.70 – 87.70 cM POPSEQ) and seven SNPs on 6H (31.90 – 92.20
521 cM POPSEQ) based on the introgressions identified from BSA. The SNPs were converted
522 to restriction enzyme-based CAPS markers for genotyping. For SNP marker mapping, we
523 phenotyped 136 new $F_{2s}$ of the Morex × *mul2.b* population in the year 2015 (POP 2015).
524 We knew that the barley spike-branching gene *COM2* is also located on 2H (45.0 cM),
525 mutants of which often displayed the LS-IN phenotype (McKim et al. 2018; Poursarebani
526 et al. 2015). To check if the LS-IN phenotype is regulated by *COM2*, we developed a CAPS
527 marker out of *COM2* for mapping in our population. Different from the phenotyping
528 method followed for POP 2014-1 and POP 2014-2, we quantified the LS-IN phenotype in
529 POP 2015, based on *mul2-I*, *-II*, *-III*, and *-IV* classes (described earlier in results). In the
530 same $F_{2s}$, we quantified the CS-SS phenotype. Out of 136 $F_{2s}$ phenotyped, 67 showed

531 various quantities of *mul2-I, -II, -III, -IV* LS-IN phenotypes, while 69 were wildtype for LS-
532 IN. This segregation did not fit the incomplete dominant inheritance ($\chi 2$ = 48.039, *p-value*
533 = <0.0001) observed in POP 2014-1 and POP 2014-2, sugesting some sort of plasticity for
534 the LS-IN phenotype. With respect to the CS-SS phenotype, 62 $F_{2s}$ of POP 2014-1 showed
535 the CS-SS, the majority of which also had LS-IN phenotype while 74 were wt for CS-SS.
536
537 For linkage analysis of the LS-IN phenotype, we converted the phenotype quantities
538 (cumulative frequencies of the *mul2-I, -II, -III,* and *-IV* classes) into binary scores along
539 with SNP marker genotypes. However, after comparing the SNP and phenotype marker
540 scores, six out of 136 $F_{2s}$ had a mismatch between phenotype and marker genotypes.
541 These included, two $F_{2s}$ that showed the LS-IN phenotype but had homozygous WT
542 genotype calls and four $F_{2s}$ that were phenotypically wt for LS-IN but had mutant
543 genotype calls at the majority of markers mapped on 2H (**Fig. 6A**). The two $F_{2s}$ that had
544 wt genotype calls on 2H showed a weak LS-IN phenotype (*mul2-III* and *-IV*; **Fig. 6A**).
545 However, performing linkage analysis of the LS-IN phenotype and genotype scores by
546 excluding the six conflicting $F_{2s}$, linked LS-IN in between markers M1865727 and M5729
547 away from the *COM2* gene (**Fig. 6B**). Since the LS-IN phenotype was measured in a
548 quantitative manner, we were also able to perform QTL analysis for the LS-IN phenotype
549 (cumulative *mul2.b-I, -II, -III, and -IV*) together with CAPS marker data from 2H and 6H.
550 Expectedly based on our previous exome capture data, LS-IN showed a major QTL on 2H
551 with marker M5729 explaining the highest phenotypic value (**Fig. 6C, E**). However, we
552 also noticed another major QTL for the LS-IN phenotype on 6H with FL209450 explaining
553 the highest phenotypic value (**Fig. 6C, E**). Furthermore, our QTL analysis of the CS-SS
554 phenotype with marker data from 2H and 6H showed a single major QTL on 6H (**Fig. 6D-**
555 **E**). Most interestingly, the CS-SS QTL co-located with the QTL region identified for LS-IN
556 on 6H (**Fig. 6C-E**), indicating that the 6H locus may regulate both phenotypes—CS-SS and
557 LS-IN.
558
559 ***Whole-genome QTL analysis reveals more and novel genetic factors conditioning the***
560 ***LS-IN and CS-SS phenotypes***
561 Since our partial-genome QTL analysis of LS-IN and CS-SS in the Morex × *mul2.b*
562 population (POP 2015) indicated that these phenotypes are probably inherited in a
563 quantitative fashion, we intended to perform whole-genome QTL analysis in the Morex ×
564 *mul2.b* $F_2$ population. To this end, we screened another ~1,000 $F_{2s}$ with markers M9646

565 and M41923 on 2H that are spaced apart by 37.8 cM (**Fig. 6B**). Between these two
566 markers, we selected 177 recombinant individuals as an independent $F_2$ population (POP
567 2016). We quantified their LS-IN and CS-SS phenotypes by counting the instances of LS-
568 IN (cumulatively, number of *mul2-I, -II, -III,* and *-IV* classes) and CS-SS (extra central
569 spikelets) per plant.
570
571 The LS-IN phenotype scored in POP 2016 fitted an incomplete dominant inheritance
572 mode as observed in POP 2014-1 ($\chi 2 = 0.092$; p-value = 0.761). With respect to the CS-SS
573 phenotype in POP 2016, 38 $F_{2s}$ did not show a phenotype, whereas 138 $F_{2s}$ carried the CS-
574 SS phenotype. The majority of the $F_{2s}$ harboring the CS-SS phenotype also had the LS-IN
575 phenotype (104 $F_{2s}$). The frequencies of phenotype distributions were also skewed for the
576 LS-IN and CS-SS phenotypes, indicating that these traits were not strictly polygenic (**Fig.**
577 **S5**). In spite of that, we proceeded analyzing LS-IN and CS-SS as quantitative traits, since
578 we had observed two QTLs (on 2H and 6H chromosomes) for the LS-IN trait in the POP
579 2015. For the QTL analysis of $F_{2s}$ in POP 2016, we normalized the phenotypic value of both
580 traits (LS-IN and CS-SS) by estimating BLUEs to have a more meaningful view of the
581 phenotypes on a per spike basis.
582
583 The 177 $F_{2s}$ from POP 2016 were subjected to genotyping by sequencing (GBS) to
584 generate SNP marker data. From our GBS analysis we got data for 1,573 high-quality SNP
585 markers. Upon filtering for markers with >10% missing data or two or more linked
586 markers without recombination across $F_{2s}$, we mapped 605 markers onto 11 linkage
587 groups. The barley chromosome 3H was split into three linkage groups, whereas 5H, 7H
588 were split into two linkage groups due to lack of marker coverage mainly in the
589 centromeric regions. Chromosomes 1H, 2H, 4H, and 6H formed unique linkage groups
590 (**Supplementary table 3**). The genotypic and phenotypic data were used for QTL
591 detection using Genstat 19.
592
593 Similar to the QTLs identified from POP 2015, we identified two major QTLs for LS-IN
594 (cumulative *mul2.b-I, -II, -III, and -IV*) on 2H (termed *QMUL2.I-IV.ipk-2H*; -log10(P)–24.70;
595 %PVE–32.19) and 6H (*QMUL2.I-IV.ipk-6H*; -log10(P)–10.93; %PVE–13.50) (**Fig. 7; Table**
596 **1**) in POP 2016. We also performed QTL analysis for the LS-IN component classes *mul2.b-*
597 *I, -II, -III, and –IV* separately to further dissect the genetic basis of the individual phenotype
598 classes. For the *mul2-I, -II,* and *-III* classes major QTLs were detected on 2H and 6H which

599 co-located with *QMUL2.I-IV.ipk-2H* and *QMUL2.I-IV.ipk-6H* (**Fig. 7; Table 1**). For the
600 weakest LS-IN component class - *mul2.b-IV*, only the 2H QTL co-located with both LS-IN
601 cumulative and component QTLs on 2H while the 6H QTL was not detected for this class
602 (**Fig. 7; Table 1**). Apart from the 2H and 6H QTLs for the *mul2.b-III* LS-IN component class,
603 we identified two minor QTLs, *QMUL2.III.ipk-3H(1)* and *QMUL2.III.ipk-3H(2)* on 3H(1) and
604 3H(2) linkage groups explaining 8.43% and 5.65% of the observed phenotypic variation
605 (**Fig. 7; Table 1**). Notably, in four out of five QTLs detected for the LS-IN trait the high
606 phenotype value allele was derived from the *mul2.b* mutant parent; except for
607 *QMUL2.III.ipk-3H(2)*, here the high-value allele was derived from Morex (**Fig. S6D**).
608
609 For the CS-SS trait a single major QTL on 6H was identified (*QMUL2.SS.ipk-6H*; -log10(P)–
610 26.38; %PVE – 47.11; **Fig. 7; Table 1**). Interestingly, *QMUL2.SS.ipk-6H* co-located with
611 *QMUL2.I-IV.ipk-6H* and also with the 6H QTLs for LS-IN component classes, *mul2-I, -II,* and
612 *-III* (**Fig.7**), indicating that a single genetic factor may underlie the LS-IN and CS-SS QTLs
613 on 6H. We also found a minor QTL for the CS-SS trait on 5H(2) - *QMUL2.AS.ipk-5H(2)*
614 explaining 4.32% of phenotypic variation (**Fig. 7; Table 1**). Interestingly, the high
615 phenotype value allele for *QMUL2.AS.ipk-5H(2)* originated from the Morex parent (**Fig.**
616 **S7B**). Thus, the Morex-derived high phenotype value alleles of minor QTLs, *QMUL2.III.ipk-*
617 *3H(2)* for LS-IN and *QMUL2.AS.ipk-5H(2)* for CS-SS showed that independent genetic
618 factors responsible for controlling these traits are present in both parents of the Morex ×
619 *mul2.b* cross.
620
621 ***QTL allele effects for the LS-IN and CS-SS phenotypes***
622 To estimate the phenotypic effect contributed by QTL alleles for the LS-IN trait, we
623 evaluated combinations of Morex ("AA"), *mul2.b* (allele "*aa*"), and Morex/*mul2.b* (alleles
624 "*A/a*") alleles at *QMUL2.I-IV.ipk-2H* and *QMUL2.I-IV.ipk-6H* QTLs in $F_2$. Interestingly, the
625 strongest mutant LS-IN phenotype (cumulative *mul2.b-I, -II, -III, and -IV*) was manifested
626 only in $F_{2s}$ with mutant "*aa*" alleles present in both QTL loci (**Fig. S8A**). The LS-IN
627 phenotypic effect got drastically reduced in $F_{2s}$ with alleles "*aa*" and "*AA*" at 2H and 6H
628 QTLs, respectively (**Fig. S8A**). Also heterozygosity at both QTL loci in combination with
629 the respective mutant "*aa*" allele [e.g. *aa*(2H)/*Aa*(6H); or *Aa*(2H)/*aa*(6H)] enhanced LS-
630 IN phenotype in comparison with the wild type allele combination, [(e.g. *aa*(2H)/*AA*(6H)
631 or *AA*(2H)/*aa*(6H)] indicating that *QMUL2.I-IV.ipk-6H* enhanced *QMUL2.I-IV.ipk-2H* effect
632 in an additive manner (**Fig. S8A**). The single major QTL for the CS-SS trait (*QMUL2.SS.ipk-*

633 *6H*), however, was not influenced by the alleles at *QMUL2.I-IV.ipk-2H*, indicating that the
634 CS-SS trait is majorly controlled by 6H QTL **(Fig. S8B**). Similar phenotypic effects for LS-
635 IN and CS-SS traits were also observed in $F_{2:3}$ generation (**Fig. S9**), indicating the stable
636 inheritance of these phenotypes.
637
638 The LS-IN component trait *mul2.b-III* had two major QTLs, one each on 2H (*QMUL2.III.ipk-*
639 *2H*) and 6H (*QMUL2.III.ipk-6H*) but also two minor QTLs on 3H (*QMUL2.III.ipk-3H(1)*,
640 *QMUL2.III.ipk-3H(2)*). Interestingly, the phenotypic effect was highly enhanced in $F_{2s}$ with
641 favorable QTL alleles at these four loci, i.e. *mul2.b* allele at 2H, 6H, 3H(1) QTLs, and Morex
642 allele at 3H(2) QTL, indicating the additivity of these loci (**Fig. S6**). Also for the CS-SS trait,
643 a similar additive phenotype was observed in $F_2$ individuals carrying high phenotype
644 value alleles at *QMUL2.SS.ipk-6H* (*mul2.b* alleles) and *QMUL2.SS.ipk-5H(2)* (Morex alleles)
645 loci (**Fig. S7**.)
646
647 **Discussion**
648 ***Mutations in multiflorus.2b induce two ancestral phenotypes – LS-IN and CS-SS***
649 The spikes of the *Triticeae* tribe are proposed to be derivatives of ancestral compound
650 spike/panicle inflorescences obtained through an evolutionary series of inflorescence
651 branch complexity reduction (Koppolu and Schnurbusch 2019; Perreta et al. 2009;
652 Vegetti 1995). Within Triticeae species, spike inflorescences show structural differences
653 in terms of determinacy at the levels of the spike (presence or absence of terminal
654 spikelet) and spikelet (uni- or multi-floreted spikelet) (Sakuma et al. 2011). The uni-
655 floreted condition is manifested due to suppression of rachilla elongation after the
656 initiation of the first floret, whereas in multi-floreted spikelets rachilla elongation
657 continues to generate more florets. Two peculiar Triticeae species with contrasting
658 determinacy features at both levels include barley (determinate spikelet, indeterminate
659 spike) and wheat (determinate spike, indeterminate spikelet). It was proposed that
660 terminal spikelet identity (determinate spike) and multi-floreted conditions
661 (indeterminate spikelet) of wheat are ancestral, whereas indeterminate spike and uni-
662 floreted (determinate spikelet) conditions are derived features in barley (Clayton 1990;
663 Zhong et al. 2021). The mutants of barley *mul2.b* lost the spikelet determinacy producing
664 ancestral multi-floreted condition similar to wheat spikelets, but the derived spike
665 indeterminacy character is retained. Interestingly the multi-floreted condition was
666 restricted to LS of *mul2.b* (LS-IN) with CSs retaining the determinate character. Such

667 determinacy differences between CS and adjacent LSs could be probably due to separate
668 genetic factors controlling this condition in CS and LS differently.
669
670 Notably, mutants of *mul2.b* also produce supernumerary spikelets (SS) in the CS (CS-SS).
671 The SS feature appears to be analogous with the paired spikelet phenotype of wheat and
672 the spikelet pair phenotype characteristic to maize, sorghum, and other *Andropogoneae*
673 species (Boden et al. 2015). Also, species belonging to the Triticeae genera *Crithops* and
674 *Taeniatherum* bear two spikelets at each rachis node on the spike (Frederiksen and
675 Seberg 1992), probably indicating that the mechanism regulating SS phenotype is an
676 ancestral feature retained in some of the *Triticeae* species. However, the CS-SS phenotype
677 in *mul2.b* and *flo.a* could be potentially a revertant ancestral phenotype due to mutations
678 in respective loci.
679
680 ***LS-IN and CS-SS are quantitatively inherited in the Morex × mul2.b* cross**
681 Based on our in-depth phenotypic analysis we showed that the *mul2.b* phenotype is a
682 combination of rachilla elongation in LSs (LS-IN) and supernumerary spikelet formation
683 in CSs (CS-SS). The previous genetic and phenotypic analyses involving *mul2.b* apparently
684 did not consider the CS-SS phenotype in central spikelets. Also, the LS-IN phenotype was
685 not evaluated in sufficient detail probably owing to difficulties in visualizing the rachilla
686 elongation in lateral spikelets. This might have potentially lead to the classification of
687 *mul2.b* as a monogenic recessive locus (Walker et al. 1963). Our QTL analysis based on
688 comprehensive LS-IN and CS-SS phenotypes revealed two major QTLs for LS-IN (*QMUL2.I-*
689 *IV.ipk-2H, QMUL2.I-IV.ipk-6H*) and one major QTL for the CS-SS phenotype (*QMUL2.SS.ipk-*
690 *6H*) (**Fig. 7; Table 1**). Also, two minor QTLs for LS-IN [*QMUL2.III.ipk-3H(1), QMUL2.III.ipk-*
691 *3H(2)*] and one for CS-SS phenotype [*QMUL2.SS.ipk-5H(2)*] were identified indicating the
692 quantitative nature of the *mul2.b* phenotypes (**Fig. 7; Table 1**). It should be noted that the
693 cv. Morex (wt parent) occasionally showed mild and infrequent rachilla elongation in LSs
694 as well as supernumerary spikelet formation in CS (data not shown). Consistent with this,
695 we observed for each trait one minor QTL, *QMUL2.III.ipk-3H(2)* and *QMUL2.SS.ipk-5H(2)*,
696 where the phenotypic high-value allele was derived from Morex (**Fig. 7; Table 1**).
697 Previous genetic analyses in wheat involving the paired spikelet phenotype (analogous to
698 *mul2.b* CS-SS) also reported quantitative variation for this trait (Boden et al. 2015;
699 Dobrovolskaya et al. 2015; Echeverry-Solarte et al. 2014).
700

701 Our genetic analysis of LS-IN and CS-SS phenotypes revealed co-locating QTLs on 6H
702 (*QMUL2.I-IV.ipk-6H, QMUL2.SS.ipk-6H*; **Fig. 7**), indicating that these phenotypes are
703 potentially regulated by a single locus on 6H. On top of that, the phenotypic effect of LS-
704 IN QTL on 2H is significantly enhanced by the 6H QTL alleles in an additive manner,
705 without which, the LS-IN phenotypic was drastically reduced (**Fig. S7**). Interestingly, the
706 Bowman near-isogenic line of *mul2.b* (BM-NIL(*mul2.b*); GSHO 2089, BW607) showed a
707 mild LS-IN phenotype, whereas the CS-SS phenotype is completely missing in BM-
708 NIL(*mul2.b*) (**Fig. S10**). Such a mild LS-IN phenotype and lack of CS-SS phenotype in BM-
709 NIL(*mul2.b*) could be probably due to the lack of *mul2.b* 6H introgression from the
710 original mutant that enhances the phenotypic effect of 2H QTL. For the LS-IN phenotype
711 component phenotype class *mul2.b-III* we also identified two minor QTLs on 3H. Thus, our
712 precise phenotype quantification data guided us to genetically dissect genomic regions
713 responsible for various LS-IN phenotypes.
714

715 ***Conclusion***

716 Yield in small grain cereals such as barley and wheat is mainly contributed by the number
717 of grains produced per unit area (Ferrante et al. 2017; García et al. 2015; Sakuma and
718 Schnurbusch 2020; Serrago et al. 2013). The grain number can be improved by increasing
719 spikelet number per spike, floret number per spikelet and also enhancing floret fertility
720 within spikelets. Here we characterized a barley mutant, *mul2.b*, that showed multi-
721 floreted spikelets as well as more spikelets per spike (supernumerary spikelet formation).
722 Through our genetic analysis, we identified component QTLs conditioning these two trait
723 phenotypes. Further, we laid the foundation for identifying and characterizing the genetic
724 factors underlying these phenotypes by QTL cloning in the future.
725

726 ***Acknowledgments***

727 The authors thank Udda Lundqvist, Jerome Franckowiak, and Thirulogachandar
728 Venkatasubbu for the insightful discussions on the *multiflorus2.b* mutant. We thank
729 Harold Bockelman (USDA-ARS, USA) for providing the *multiflorus2.b* and Montcalm
730 germplasm. We thank Roopkamal Kaur for help with the data analysis. We thank Corinna
731 Trautewig, Mechthild Pürschel, Angelika Pueschel, Kerstin Wolf, Susanne König and
732 Manuela Knauft for excellent technical assistance. We thank Anne Fiebig for GBS and
733 exome capture sequence data submission. We are also thankful to Heike Müller and
734 Andreas Bähring for supporting graphical artwork.

735 ***Funding***

736 This study received financial support from the Chinese Scholarship Council (CSC) to G.J.
737 The Schnurbusch laboratory was supported by the HEISENBERG Program of the German
738 Research Foundation (DFG) (grant nos. SCHN 768/8-1 and SCHN 768/15-1), the
739 European Research Council (ERC) (grant agreement no. 681686 "LUSH SPIKE"), ERC-
740 2015-CoG, and IPK core budget.

741

742 ***Conflicts of interest***

743 Authors declare no conflicts of interest.

744

745 ***Availability of data and material***

746 The sequence data generated in this study can be accessed from European Nucleotide
747 Achive (ENA) under the accession numbers PRJEB44305 (exome capture) and
748 PRJEB44306 (GBS).

749

750 ***Authors' contributions***

751 R.K. conceptualized the study together with T.S.; T.S. and R.K. jointly supervised the study.
752 R.K. generated mapping populations and established the *mul2.b* phenotyping
753 methodology. R.K. and G.J. conducted phenotypic and genetic analyses. Q.H.M. generated
754 BLUE scores for POP 2016. S.G.M. conducted GBS data analysis for POP 2016. T.R.
755 conducted scanning electron microscopy of immature barley spikes. A.H. and N.S.
756 provided expertise and resources for exome capture and GBS experiments. M.M.
757 conducted exome capture data analysis for POP 2014. R.K. drafted the MS with the help
758 from T.S. All authors read and approved the MS.

759

760 ***References***

761 Amagai Y, Aliyeva AJ, Aminov NK, Martinek P, Watanabe N, Kuboyama T (2014) Microsatellite mapping
762 of the genes for sham ramification and extra glume in spikelets of tetraploid wheat. Genetic
763 Resources and Crop Evolution 61:491-498
764 Bates D, Mächler M, Bolker B, Walker S (2015) Fitting Linear Mixed-Effects Models Using lme4. Journal
765 of statistical software 67:48
766 Boden SA, Cavanagh C, Cullis BR, Ramm K, Greenwood J, Jean Finnegan E, Trevaskis B, Swain SM (2015)
767 *Ppd-1* is a key regulator of inflorescence architecture and paired spikelet development in wheat.
768 Nature Plants 1:14016
769 Bonnett OT (1935) The development of the barley spike. Journal of Agricultural Research 51:451-460
770 Bonnett OT (1936) The development of the wheat spike. Journal of Agricultural Research 53:445-451
771 Bonnett OT (1966) Inflorescences of maize, wheat, rye, barley, and oats: their initiation and
772 development/ 721. University of Illinois, College of Agriculture, Agricultural Experiment Station

773 Bull H, Casao MC, Zwirek M, Flavell AJ, Thomas WTB, Guo W, Zhang R, Rapazote-Flores P, Kyriakidis S,
774 Russell J, Druka A, McKim SM, Waugh R (2017) Barley *SIX-ROWED SPIKE3* encodes a putative
775 Jumonji C-type H3K9me2/me3 demethylase that represses lateral spikelet fertility. Nature
776 Communications 8:936
777 Chuck G, Meeley R, Hake S (2008) Floral meristem initiation and meristem cell fate are regulated by
778 the maize *AP2* genes *ids1* and *sid1*. Development 135:3013-3019
779 Chuck G, Meeley R, Irish E, Sakai H, Hake S (2007) The maize *tasselseed4 microRNA* controls sex
780 determination and meristem cell fate by targeting *Tasselseed6/indeterminate spikelet1*. Nature
781 Genetics 39:1517-1521
782 Chuck G, Meeley RB, Hake S (1998) The control of maize spikelet meristem fate by the *APETALA2-like*
783 gene *indeterminate spikelet1*. Genes & Development 12:1145-1154
784 Clayton WD (1990) The spikelet. In: Chapman GP (ed) Reproductive versatility in the grasses.
785 Cambridge University Press, Cambridge, UK
786 Debernardi JM, Lin H, Chuck G, Faris JD, Dubcovsky J (2017) *microRNA172* plays a crucial role in wheat
787 spike morphogenesis and grain threshability. Development 144:1966-1975
788 Dixon LE, Greenwood JR, Bencivenga S, Zhang P, Cockram J, Mellers G, Ramm K, Cavanagh C, Swain
789 SM, Boden SA (2018) *TEOSINTE BRANCHED1* regulates inflorescence architecture and
790 development in bread wheat (*Triticum aestivum* L.). The Plant Cell
791 Dobrovolskaya O, Pont C, Sibout R, Martinek P, Badaeva E, Murat F, Chosson A, Watanabe N, Prat E,
792 Gautier N, Gautier V, Poncet C, Orlov YL, Krasnikov AA, Bergès H, Salina E, Laikova L, Salse J (2015)
793 *FRIZZY PANICLE* drives supernumerary spikelets in bread wheat. Plant Physiology 167:189-199
794 Druka A, Franckowiak J, Lundqvist U, Bonar N, Alexander J, Houston K, Radovic S, Shahinnia F,
795 Vendramin V, Morgante M, Stein N, Waugh R (2011) Genetic dissection of barley morphology
796 and development. Plant Physiolology 155:617-627
797 Echeverry-Solarte M, Kumar A, Kianian S, Mantovani EE, Simsek S, Alamri MS, Mergoum M (2014)
798 Genome-wide genetic dissection of supernumerary spikelet and related traits in common wheat.
799 The Plant Genome 7:plantgenome2014.2003.0013
800 Ferrante A, Cartelle J, Savin R, Slafer GA (2017) Yield determination, interplay between major
801 components and yield stability in a traditional and a contemporary wheat across a wide range of
802 environments. Field Crops Research 203:114-127
803 Frederiksen S, Seberg O (1992) Phylogenetic analysis of the Triticeae (Poaceae). Hereditas 116:15-19
804 García GA, Dreccer MF, Miralles DJ, Serrago RA (2015) High night temperatures during grain number
805 determination reduce wheat and barley grain yield: a field study. Global Change Biology 21:4153-
806 4164
807 Greenwood JR, Finnegan EJ, Watanabe N, Trevaskis B, Swain SM (2017) New alleles of the wheat
808 domestication gene *Q* reveal multiple roles in growth and reproductive development.
809 Development 144:1959-1965
810 Jeon J-S, Jang S, Lee S, Nam J, Kim C, Lee S-H, Chung Y-Y, Kim S-R, Lee YH, Cho Y-G, An G (2000) *leafy*
811 *hull sterile1* Is a homeotic mutation in a rice *MADS BOX* gene affecting rice flower development.
812 Plant Cell 12:871-884
813 Kellogg E, Camara P, Rudall P, Ladd P, Malcomber S, Whipple C, Doust A (2013) Early inflorescence
814 development in the grasses (Poaceae). Frontiers in Plant Science 4
815 Komatsuda T, Pourkheirandish M, He C, Azhaguvel P, Kanamori H, Perovic D, Stein N, Graner A, Wicker
816 T, Tagiri A, Lundqvist U, Fujimura T, Matsuoka M, Matsumoto T, Yano M (2007) Six-rowed barley
817 originated from a mutation in a homeodomain-leucine zipper I-class homeobox gene.
818 Proceedings of the National Academy of Sciences 104:1424-1429
819 Koppolu R, Anwar N, Sakuma S, Tagiri A, Lundqvist U, Pourkheirandish M, Rutten T, Seiler C,
820 Himmelbach A, Ariyadasa R, Youssef HM, Stein N, Sreenivasulu N, Komatsuda T, Schnurbusch T
821 (2013) *Six-rowed spike4* (*Vrs4*) controls spikelet determinacy and row-type in barley. Proceedings
822 of the National Academy of Sciences 110:13198-13203
823 Koppolu R, Schnurbusch T (2019) Developmental pathways for shaping spike inflorescence
824 architecture in barley and wheat. Journal of Integrative Plant Biology 61:278-295

825 Lee DY, An G (2012) Two AP2 family genes, *SUPERNUMERARY BRACT* (*SNB*) and *OsINDETERMINATE*
826 *SPIKELET 1* (*OsIDS1*), synergistically control inflorescence architecture and floral meristem
827 establishment in rice. Plant J 69
828 Lee DY, Lee J, Moon S, Park SY, An G (2007) The rice heterochronic gene *SUPERNUMERARY BRACT*
829 regulates the transition from spikelet meristem to floral meristem. Plant J 49
830 Li H (2011) A statistical framework for SNP calling, mutation discovery, association mapping and
831 population genetical parameter estimation from sequencing data. Bioinformatics 27:2987-2993
832 Li H (2013) Aligning sequence reads, clone sequences and assembly contigs with BWA-MEM. Preprint
833 at https://arxivorg/abs/13033997
834 Li H, Handsaker B, Wysoker A, Fennell T, Ruan J, Homer N, Marth G, Abecasis G, Durbin R, Subgroup
835 GPDP (2009) The sequence alignment/map format and SAMtools. Bioinformatics 25:2078-2079
836 Lolas IB, Himanen K, Gronlund JT, Lynggaard C, Houben A, Melzer M, Van Lijsebettens M, Grasser KD
837 (2010) The transcript elongation factor *FACT* affects Arabidopsis vegetative and reproductive
838 development and genetically interacts with *HUB1/2*. Plant J 61:686-697
839 Lundqvist U, Franckowiak JD (2015) *Extra floret-a*. Barley Genetics Newsletter 45:116
840 Martin M (2011) Cutadapt removes adapter sequences from high-throughput sequencing reads.
841 EMBnetjournal 17:3
842 Mascher M, Gundlach H, Himmelbach A, Beier S, Twardziok SO, Wicker T, Radchuk V, Dockter C, Hedley
843 PE, Russell J, Bayer M, Ramsay L, Liu H, Haberer G, Zhang X-Q, Zhang Q, Barrero RA, Li L, Taudien
844 S, Groth M, Felder M, Hastie A, Šimková H, Staňková H, Vrána J, Chan S, Muñoz-Amatriaín M,
845 Ounit R, Wanamaker S, Bolser D, Colmsee C, Schmutzer T, Aliyeva-Schnorr L, Grasso S, Tanskanen
846 J, Chailyan A, Sampath D, Heavens D, Clissold L, Cao S, Chapman B, Dai F, Han Y, Li H, Li X, Lin C,
847 McCooke JK, Tan C, Wang P, Wang S, Yin S, Zhou G, Poland JA, Bellgard MI, Borisjuk L, Houben
848 A, Doležel J, Ayling S, Lonardi S, Kersey P, Langridge P, Muehlbauer GJ, Clark MD, Caccamo M,
849 Schulman AH, Mayer KFX, Platzer M, Close TJ, Scholz U, Hansson M, Zhang G, Braumann I,
850 Spannagl M, Li C, Waugh R, Stein N (2017) A chromosome conformation capture ordered
851 sequence of the barley genome. Nature 544:427-433
852 Mascher M, Jost M, Kuon J-E, Himmelbach A, Aßfalg A, Beier S, Scholz U, Graner A, Stein N (2014)
853 Mapping-by-sequencing accelerates forward genetics in barley. Genome Biology 15:R78
854 Mascher M, Richmond TA, Gerhardt DJ, Himmelbach A, Clissold L, Sampath D, Ayling S, Steuernagel B,
855 Pfeifer M, D'Ascenzo M, Akhunov ED, Hedley PE, Gonzales AM, Morrell PL, Kilian B, Blattner FR,
856 Scholz U, Mayer KFX, Flavell AJ, Muehlbauer GJ, Waugh R, Jeddeloh JA, Stein N (2013) Barley
857 whole exome capture: a tool for genomic research in the genus *Hordeum* and beyond. The Plant
858 Journal 76:494-505
859 McKim SM, Koppolu R, Schnurbusch T (2018) Barley Inflorescence Architecture. In: Stein N,
860 Muehlbauer GJ (eds) The Barley Genome. Springer International Publishing, Cham, pp 171-208
861 Ohmori S, Kimizu M, Sugita M, Miyao A, Hirochika H, Uchida E, Nagato Y, Yoshida H (2009) *MOSAIC*
862 *FLORAL ORGANS1*, an *AGL6-Like MADS Box* gene, regulates floral organ identity and meristem
863 fate in rice. Plant Cell 21:3008-3025
864 Perreta MG, Ramos JC, Vegetti AC (2009) Development and structure of the grass inflorescence. The
865 Botanical Review 75:377-396
866 Poursarebani N, Seidensticker T, Koppolu R, Trautewig C, Gawroński P, Bini F, Govind G, Rutten T,
867 Sakuma S, Tagiri A, Wolde GM, Youssef HM, Battal A, Ciannamea S, Fusca T, Nussbaumer T, Pozzi
868 C, Börner A, Lundqvist U, Komatsuda T, Salvi S, Tuberosa R, Uauy C, Sreenivasulu N, Rossini L,
869 Schnurbusch T (2015) The genetic basis of composite spike form in barley and 'miracle-wheat'.
870 Genetics 201:155-165
871 Poursarebani N, Trautewig C, Melzer M, Nussbaumer T, Lundqvist U, Rutten T, Schmutzer T, Brandt R,
872 Himmelbach A, Altschmied L, Koppolu R, Youssef HM, Sibout R, Dalmais M, Bendahmane A, Stein
873 N, Xin Z, Schnurbusch T (2020) COMPOSITUM 1 contributes to the architectural simplification of
874 barley inflorescence via meristem identity signals. Nature Communications 11:5138
875 Ramsay L, Comadran J, Druka A, Marshall DF, Thomas WTB, Macaulay M, MacKenzie K, Simpson C,
876 Fuller J, Bonar N, Hayes PM, Lundqvist U, Franckowiak JD, Close TJ, Muehlbauer GJ, Waugh R

877 (2011) *INTERMEDIUM-C*, a modifier of lateral spikelet fertility in barley, is an ortholog of the
878 maize domestication gene *TEOSINTE BRANCHED 1*. Nature Genetics 43:169-172
879 Ren D, Li Y, Zhao F, Sang X, Shi J, Wang N, Guo S, Ling Y, Zhang C, Yang Z, He G (2013) *MULTI-FLORET*
880 *SPIKELET1*, which encodes an AP2/ERF protein, determines spikelet meristem fate and sterile
881 lemma identity in rice. Plant Physiology 162:872-884
882 Ren D, Xu Q, Qiu Z, Cui Y, Zhou T, Zeng D, Guo L, Qian Q (2019) *FON4* prevents the multi-floret spikelet
883 in rice. Plant Biotechnology Journal 17:1007-1009
884 Ren D, Yu H, Rao Y, Xu Q, Zhou T, Hu J, Zhang Y, Zhang G, Zhu L, Gao Z, Chen G, Guo L, Zeng D, Qian Q
885 (2018) 'Two-floret spikelet' as a novel resource has the potential to increase rice yield. Plant
886 Biotechnology Journal 16:351-353
887 Sakuma S, Golan G, Guo Z, Ogawa T, Tagiri A, Sugimoto K, Bernhardt N, Brassac J, Mascher M, Hensel
888 G, Ohnishi S, Jinno H, Yamashita Y, Ayalon I, Peleg Z, Schnurbusch T, Komatsuda T (2019)
889 Unleashing floret fertility in wheat through the mutation of a homeobox gene. Proceedings of
890 the National Academy of Sciences 116:5182-5187
891 Sakuma S, Salomon B, Komatsuda T (2011) The domestication syndrome genes responsible for the
892 major changes in plant form in the Triticeae crops. Plant Cell Physiol 52:738-749
893 Sakuma S, Schnurbusch T (2020) Of floral fortune: tinkering with the grain yield potential of cereal
894 crops. New Phytologist 225:1873-1882
895 Schnurbusch T (2019) Wheat and barley biology: Towards new frontiers. Journal of Integrative Plant
896 Biology 61:198-203
897 Serrago RA, Alzueta I, Savin R, Slafer GA (2013) Understanding grain yield responses to source–sink
898 ratios during grain filling in wheat and barley under contrasting environments. Field Crops
899 Research 150:42-51
900 Simons KJ, Fellers JP, Trick HN, Zhang Z, Tai Y-S, Gill BS, Faris JD (2006) Molecular characterization of
901 the major wheat domestication gene *Q*. Genetics 172:547-555
902 Spitzer M, Wildenhain J, Rappsilber J, Tyers M (2014) BoxPlotR: a web tool for generation of box plots.
903 Nature Methods 11:121-122
904 Tanaka W, Toriba T, Ohmori Y, Yoshida A, Kawai A, Mayama-Tsuchida T, Ichikawa H, Mitsuda N, Ohme-
905 Takagi M, Hirano H-Y (2012) The *YABBY* gene *TONGARI-BOUSHI1* is involved in lateral organ
906 development and maintenance of meristem organization in the rice spikelet. The Plant Cell
907 24:80-95
908 van Esse GW, Walla A, Finke A, Koornneef M, Pecinka A, von Korff M (2017) *SIX-ROWED SPIKE3* (*VRS3*)
909 is a histone demethylase that controls lateral spikelet development in barley. Plant Physiology
910 174:2397-2408
911 Vegetti AA, A.M. (1995) Some evolution trends in the inflorescence of Poaceae. Flora 190:225-228
912 Voorrips RE (2002) MapChart: Software for the graphical presentation of linkage maps and QTLs.
913 Journal of Heredity 93:77-78
914 Waddington SR, Cartwright PM, Wall PC (1983) A quantitative scale of spike initial and pistil
915 development in barley and wheat. Annals of Botany 51:119-130
916 Walker GWR, Dietrich J, Miller R, Kasha K (1963) Recent barley mutants and their linkages II. Genetic
917 data for further mutants. Canadian Journal of Genetics and Cytology 5:200-219
918 Wendler N, Mascher M, Nöh C, Himmelbach A, Scholz U, Ruge-Wehling B, Stein N (2014) Unlocking the
919 secondary gene-pool of barley with next-generation sequencing. Plant Biotechnology Journal
920 12:1122-1131
921 Wolde GM, Trautewig C, Mascher M, Schnurbusch T (2019) Genetic insights into morphometric
922 inflorescence traits of wheat. Theoretical and Applied Genetics 132:1661-1676
923 Youssef HM, Eggert K, Koppolu R, Alqudah AM, Poursarebani N, Fazeli A, Sakuma S, Tagiri A, Rutten T,
924 Govind G, Lundqvist U, Graner A, Komatsuda T, Sreenivasulu N, Schnurbusch T (2017) *VRS2*
925 regulates hormone-mediated inflorescence patterning in barley. Nature Genetics 49:157-161
926 Zhang T, Li Y, Ma L, Sang X, Ling Y, Wang Y, Yu P, Zhuang H, Huang J, Wang N, Zhao F, Zhang C, Yang Z,
927 Fang L, He G (2017) *LATERAL FLORET 1* induced the three-florets spikelet in rice. Proceedings of
928 the National Academy of Sciences 114:9984-9989

929 Zhong J, van Esse GW, Bi X, Lan T, Walla A, Sang Q, Franzen R, von Korff M (2021) *INTERMEDIUM-M*
930 encodes an *HvAP2L-H5* ortholog and is required for inflorescence indeterminacy and spikelet
931 determinacy in barley. Proceedings of the National Academy of Sciences 118:e2011779118

932 **Main text figures**

933 **Figure 1. Spike and spikelet phenotypes of cv. Montcalm and derived mutant**
934 ***mul2.b.***
935 (A) cv. Montcalm and *mul2.b* spikes. The dorsal triple spikelet nodes of Montcalm and
936 *mul2.b* are stripped-off in-order to visualize the rachilla of the lateral spikelets from
937 ventral nodes. The rachilla of lateral spikelets in Montcalm and the second floret on the
938 elongated rachilla of *mul2.b* are colored in yellow and blue respectively. (B) Triple-
939 spikelet node of Montcalm with rachilla of central and lateral spikelets colored in yellow.
940 (C) Triple spikelet node of *mul2.b* mutant showing the formation of the second floret in
941 lateral spikelet nodes (LS-F2). The rachilla on LS-F2 is colored in yellow. (D) The lateral
942 spikelet node of *mul2.b* showing the formation of the second (LS-F2) and third florets (LS-
943 F3). (E) A representative wheat spikelet with six visible florets (F1-F6). (F) *mul2.b* spike
944 showing additional florets in lateral spikelets (blue colored) and supernumerary spikelets
945 (green colored) on the abaxial side of primary central spikelets (indicated by yellow
946 stars). Awns in all images (except 1E) are clipped-off for better visualization of spikelet
947 features.
948
949 **Figure 2. Scanning electron micrographs highlighted with rachilla primordia in cv.**
950 **Montcalm and derived mutant *mul2.b*.**
951 (A-C) Immature spikes of cv. Montcalm at Waddington W4.0 (A), W4.5 (B), and ~W5.0 (C).
952 (D) Close-up view of three triple-spikelet nodes of Montcalm (E) Top-down view of single
953 triple-spikelet of Montcalm. The lateral spikelet rachilla primordia in figures 2A-E are
954 colored in yellow. (F-I) Immature spikes of *mul2.b* at ~W4.0 (F), W4.5(G), ~W5.0 (H), and
955 W6.0 (I). (J) Close up view of three triple-spikelet nodes of *mul2.b*. (K) Top-down view of
956 single triple-spikelet of *mul2.b*. The rachilla primordium/second floret in lateral spikelets
957 in figures 2F-K are colored in blue. The rachilla primordium seen on the second floret in
958 2I, 2J, and central spikelet in 2K is colored in yellow. All immature spikes in figure 2 are
959 staged based on the central spikelet development.
960
961 **Figure 3. Phenotype classification for lateral spikelet indeterminacy.**
962 (A) Representative spikelet-triplet showing wild-type rachilla of lateral and central
963 spikelets. (B-E) elongated lateral spikelet rachilla developing class I (B, C) and class II
964 additional florets (D, E). (F-G) Class III rachilla elongating into a thin and long filament-
965 like structure. (H-I) Class IV phenotype showing a bifurcated (H) or wedge-shaped
966 rachilla in lateral spikelets (I). Rachilla/additional florets/rachilla malformations in
967 lateral spikelets are indicated with white arrowheads. Yellow arrowheads in figure 3D
968 and E indicate a pedicel below the extra floret in lateral spikelets.
969
970 **Figure 4. Exome capture-based bulked segregant analysis in Morex × *mul2.b* (POP**
971 **2014-1).**
972 (A) Graph showing number of $F_2$ individuals per exome capture pool, number of exome
973 capture $F_2$ individuals showing supernumerary spikelet phenotype, and strength of
974 supernumerary spikelet phenotype (total supernumerary spikelets per pool) in WT and
975 mt pools. (B) Allele frequency plot showing the frequency of wild-type (Morex) and
976 mutant (*mul2.b*) allele distributions across seven barley chromosomes.
977

**Figure 5. Allelism analysis between *mul2.b* and BM-NIL(*flo.a*).**
(A-C) Supernumerary spikelet formation in BM-NIL(*flo.a*) (A), *mul2.b* (B), and the respective $F_1$ hybrid (C). (D) Supernumerary spikelet phenotypes in BM-NIL(*flo.a*) × *mul2.b* $F_2$ individuals. (E) Mode of inheritance of supernumerary spikelet phenotype in BM-NIL(*flo.a*) × *mul2.b*. Supernumerary spikelets are indicated by blue arrowheads. F – Dominant *FLO.A*; S – dominant second supernumerary spikelet locus; f – Recessive *flo.a*; s – recessive second supernumerary spikelet locus; S/s & F/f – Heterozygotes.

**Figure 6. Linkage and QTL mapping of LS-IN and CS-SS phenotypes in Morex × *mul2.b* (POP 2015).**
(A) The upper panel shows the graphical genotypes of CAPS markers (derived from 2H LS-IN introgression identified from exome capture) that are not fitting with the LS-IN phenotype shown in the lower panel. The linkage map for rachilla elongation/additional floret phenotype after omitting the six lines with genotype-phenotype conflicts reported in figure 6A**.** (C) QTLs for rachilla elongation/additional floret on 2H, 6H chromosomes. (D) QTL for supernumerary spikelet phenotype on the 6H chromosome. (E) Summary of QTLs reported in figures 6C, and D.

**Figure 7. Identified QTLs for LS-IN and CS-SS phenotypes in the Morex × *mul2.b* (POP 2016)**

**Main text tables**
**Table 1. List of identified QTLs for LS-IN and CS-SS traits in the Morex × *mul2.b* (POP 2016)**

**Supplementary figures and tables**
**Supplementary figure 1. Spike and biomass-related traits – Montcalm vs. *mul2.b*.**
(A) Maximum yield potential of Montcalm and *mul2.b* measured before anthesis. (B-C) Fertile grain-bearing spikelets (B) and sterile spikelets (C) at spike maturity. (D-G) Biomass-related traits such as plant height (D) total tillers (E), productive (F), and unproductive (G) tillers. P-values were calculated based on *Student's t-test* (two-tailed).

**Supplementary figure 2. Grain morphometry parameters – Montcalm vs. *mul2.b*.**
(A-D) Thousand-grain weight (A), grain area (B), width (C), and length (D) of Montcalm and *mul2.b* measured from central and lateral spikelet grains together. (E-H) Thousand-grain weight (E), grain area (F), width (G), and length (H) of Montcalm and *mul2.b* measured from central spikelet grains. (I-L) Thousand-grain weight (I), grain area (J), width (K), and length (L) of Montcalm and *mul2.b* measured from lateral spikelet grains. P-values were calculated based on *Student's t-test* (two-tailed).

**Supplementary figure 3. *mul2.b* phenotype classification for lateral spikelet indeterminacy.**
(A) Wild-type rachilla of Montcalm. (B-C) class I (B) and class II (C) additional florets excised from the lateral spikelets of *mul2.b*. (D-E) Malformed rachillae of Class III (D) and class IV (E) excised from lateral spikelets.

**Supplementary figure 4. Distribution of different classes of lateral spikelet indeterminacy and supernumerary spikelet phenotypes in spikes of the *mul2.b* mutant.**

1027 The yellow-colored cells at spikelet node 1 and in the upper spikelet nodes indicate the
1028 aborted spikelets at the base and top of the spike, respectively after anthesis. Cells
1029 highlighted in green indicate the fertile spikelets that potentially bear a grain. The cells in
1030 orange indicate the unfilled spikelets (spikelets formed but did not grow further). Classes,
1031 I, II, III, and IV indicate respective phenotypes for rachilla indeterminacy or additional
1032 floret formation in lateral spikelets, whereas SS is supernumerary spikelet phenotype in
1033 central spikelets. The notation "!" in the upper aborted spikelets (Yellow) indicates the
1034 absence of phenotypic information for lateral spikelet indeterminacy/additional spikelet
1035 and supernumerary spikelet phenotypes. CS – Central Spikelet; LL – Left Lateral spikelet;
1036 RL – Right Lateral spikelet; SS – Supernumerary spikelet.
1037
1038 **Supplementary figure 5. Frequency distribution of LS-IN and CS-SS phenotypes in**
1039 **Morex × *mul2.b* (POP 2016)**
1040
1041 **Supplementary figure 6.** Phenotypic effect of LS-IN trait at individual QTLs
1042 *QMUL2.III.ipk-2H* (A) *QMUL2.III.ipk-3H(1)* (B) *QMUL2.III.ipk-6H* (C) and *QMUL2.III.ipk-*
1043 *3H(2)* (D). (E) The cumulative phenotypic effect from the four QTLs for class III LS-IN
1044 phenotype. Phenotype frequencies shown in the box plots are derived from the genotypes
1045 of markers with the highest –log10 (p-value) and respective trait phenotype values.
1046 **Supplementary figure 7.** Phenotypic effect of CS-SS trait at individual QTLs
1047 *QMUL2.SS.ipk-6H* (A) and *QMUL2.SS.ipk-5H(2)* (B). (C)The cumulative phenotypic effect
1048 from both QTLs. Phenotype frequencies shown in the box plots are derived from the
1049 genotypes of markers with the highest –log10 (p-value) and respective trait phenotype
1050 values.
1051
1052 **Supplementary figure 8. Phenotypic effect of LS-IN and CS-SS QTLs in Morex ×**
1053 ***mul2.b*-$F_2$.**
1054 (A) Cumulative phenotypic effect of *QMUL2.I-IV.ipk-2H* and *QMUL2.I-IV.ipk-6H* QTL alleles
1055 (B) Cumulative phenotypic effect *QMUL2.I-IV.ipk-2H* and *QMUL2.SS.ipk-6H* QTL alleles.
1056 Phenotype frequencies shown in the box plots are derived from the genotypes of markers
1057 with the highest –log10 (p-value) and respective trait phenotype values.
1058
1059 **Supplementary figure 9.** Phenotypic effect of LS-IN (A) and CS-SS traits (B) in $F_{2:3}$
1060 progenies of Morex × *mul2.b*. The markers explaining the highest phenotypic value for the
1061 respective traits at 2H and 6H QTL were considered for the analysis.
1062
1063 **Supplementary figure 10.** CS-SS phenotype comparison beteen BM-NIL(*mul2.b*) and
1064 *mul2.b* in wildtype progenitor Montcalm.
1065
1066 **Supplementary Table 1. Sequences of primers used for marker mapping in Morex ×**
1067 ***mul2.b***
1068
1069 **Supplementary Table 2. Segregation pattern of LS-IN phenotype in Morex × *mul2.b***
1070 **populations.**
1071
1072 **Supplementary Table 3. Genetic linkage map features-Morex × MC(*mul2.b*) – POP**
1073 **2016.**
1074
1075

**Table 1. List of QTLs identified for LS-IN and CS-SS traits in Morex x mul2.b (POP 1-2016)**

| Chr. | QTL | Pos (cM) | Sig. Marker | Pos (cM)2 | Genetic Interval | -log10(P) | Add. Eff. | High Allele | Dom. Eff. | Dom. Allele | $R^2$ (%) |
|---|---|---|---|---|---|---|---|---|---|---|---|
| 2H | *QMUL2.I-IV.ipk-2H* | 83.00 | MK.2H.584.12.1 | 83.20 | 75.24 - 90.75 | 24.70 | 3.91 | *mul2.b* | 2.38 | Morex | 32.19 |
| 6H | *QMUL2.I-IV.ipk-6H* | 50.00 | MK.6H.409.61.1 | 50.10 | 24.72 - 75.27 | 10.93 | 2.53 | *mul2.b* | 1.49 | Morex | 13.50 |
| 2H | *QMUL2.I.ipk-2H* | 79.50 | MK.2H.584.12.1 | 83.20 | 58.69 - 100.30 | 10.89 | 1.61 | *mul2.b* | 1.27 | Morex | 15.20 |
| 6H | *QMUL2.I.ipk-6H* | 48.00 | MK.6H.174.77 | 48.20 | 35.36 - 60.63 | 13.93 | 1.93 | *mul2.b* | 1.56 | Morex | 21.64 |
| 2H | *QMUL2.II.ipk-2H* | 83.00 | MK.2H.584.12.1 | 83.20 | 71.20 - 94.79 | 15.69 | 0.32 | *mul2.b* | 0.26 | Morex | 22.83 |
| 6H | *QMUL2.II.ipk-6H* | 49.00 | MK.6H.400.46 | 49.90 | 0 - 114 | 4.36 | 0.17 | *mul2.b* | - | - | 6.57 |
| 2H | *QMUL2.III.ipk-2H* | 83.00 | MK.2H.584.12.1 | 83.20 | 74.40 - 91.59 | 18.75 | 1.61 | *mul2.b* | 0.75 | Morex | 29.53 |
| 6H | *QMUL2.III.ipk-6H* | 62.00 | MK.6H.522.77.1 | 62.40 | 0 - 114 | 3.88 | 0.66 | *mul2.b* | - | - | 4.98 |
| 3H | *QMUL2.III.ipk-3H(1)* | 8.00 | MK.3H.10.71 | 8.80 | 0 - 18 | 6.41 | 0.86 | *mul2.b* | - | - | 8.43 |
| 3H | *QMUL2.III.ipk-3H(2)* | 27.00 | MK.3H.581.28 | 27.70 | 0 - 27 | 4.44 | 0.70 | Morex | - | - | 5.65 |
| 2H | *QMUL2.IV.ipk-2H* | 83.00 | MK.2H.584.12.1 | 83.20 | 73.22 - 92.77 | 11.48 | 0.60 | *mul2.b* | - | - | 26.53 |
| 6H | *QMUL2.AS.ipk-6H* | 48.00 | MK.6H.174.77 | 48.20 | 42.97 - 53.03 | 26.38 | 1.24 | *mul2.b* | 0.73 | Morex | 47.11 |
| 5H | *QMUL2.AS.ipk-5H(2)* | 13.00 | MK.5H.602.48 | 13.80 | 0 - 66 | 3.76 | 0.38 | Morex | - | - | 4.32 |

# Figure 1

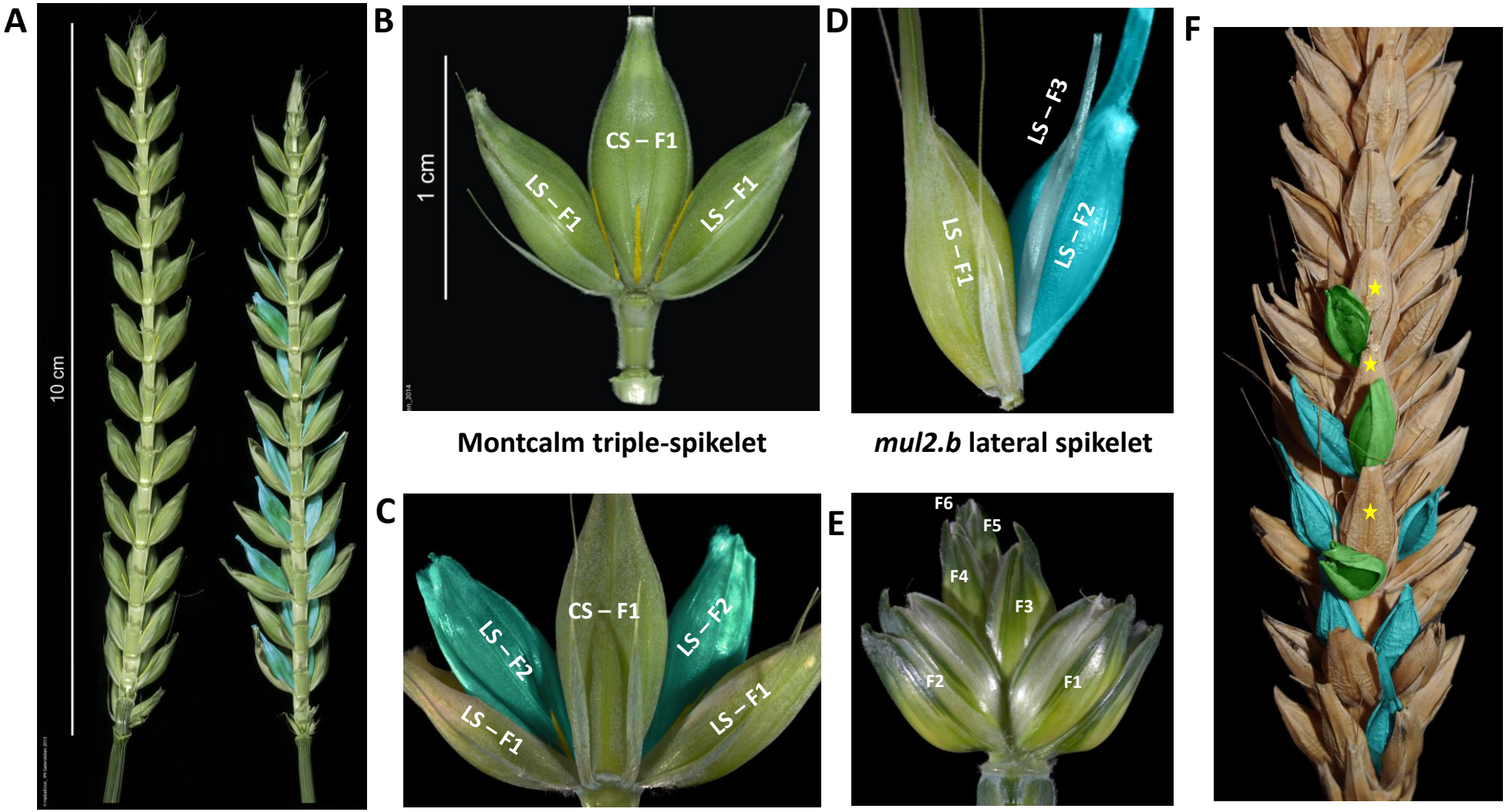
A
10 cm
Montcalm
mul2.b
B
1 cm
CS – F1
LS – F1
LS – F1
Montcalm triple-spikelet
C
CS – F1
LS – F2
LS – F2
LS – F1
LS – F1
mul2.b triple-spikelet
D
LS – F3
LS – F1
LS – F2
mul2.b lateral spikelet
E
F6
F5
F4
F3
F2
F1
Wheat spikelet cv.Mulan
F
mul2.b

# Figure 2

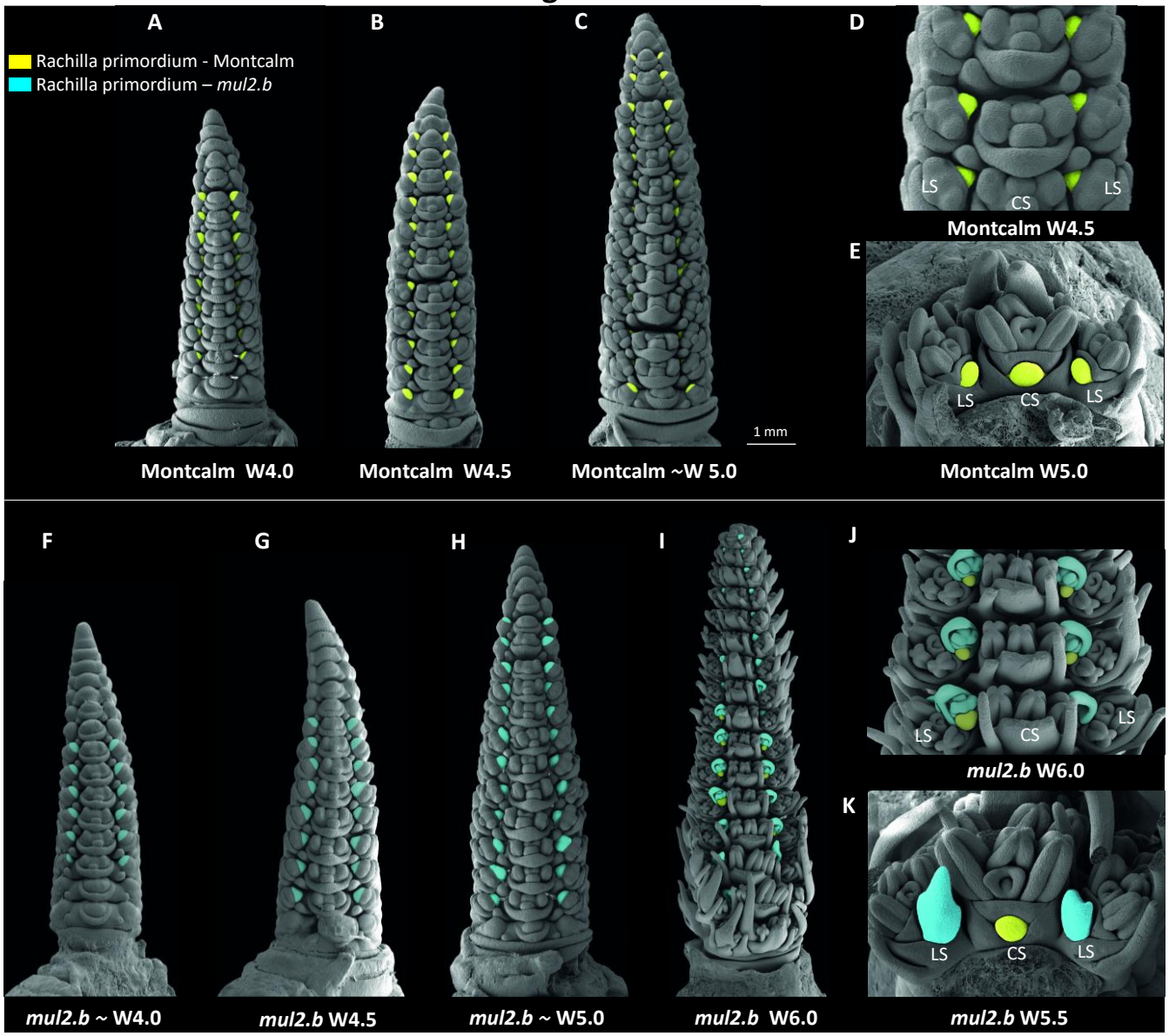
A
B
C
D
E
Rachilla primordium - Montcalm
Rachilla primordium – mul2.b
LS
CS
LS
Montcalm W4.5
LS
CS
LS
1 mm
Montcalm W4.0
Montcalm W4.5
Montcalm ~W 5.0
Montcalm W5.0
F
G
H
I
J
K
LS
CS
LS
mul2.b W6.0
LS
CS
LS
mul2.b ~ W4.0
mul2.b W4.5
mul2.b ~ W5.0
mul2.b W6.0
mul2.b W5.5

# Figure 3

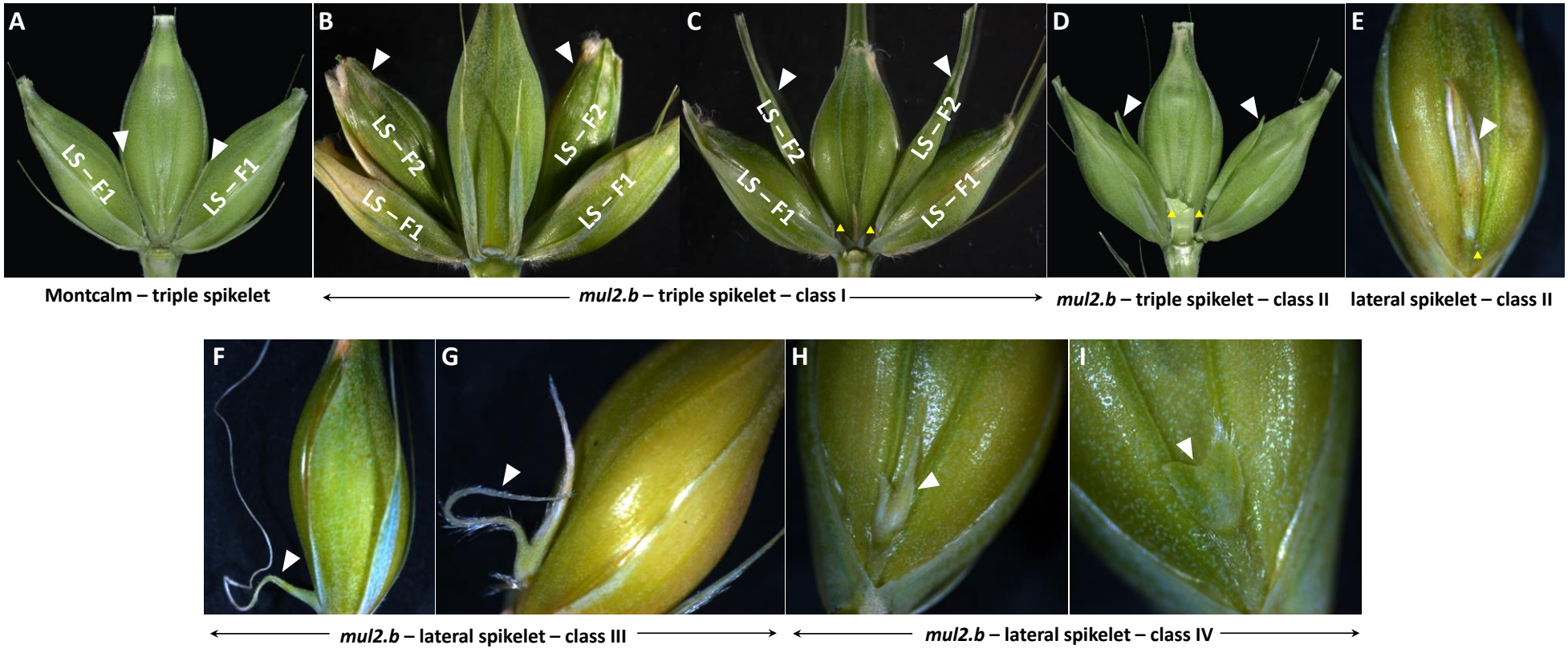
A
B
C
D
E
LS – E1
LS – F1
LS – F2
LS – F1
LS – F2
LS – F2
LS – F1
LS – F1
Montcalm – triple spikelet
mul2.b – triple spikelet – class I
mul2.b – triple spikelet – class II
lateral spikelet – class II
F
G
H
I
mul2.b – lateral spikelet – class III
mul2.b – lateral spikelet – class IV

# Figure 4

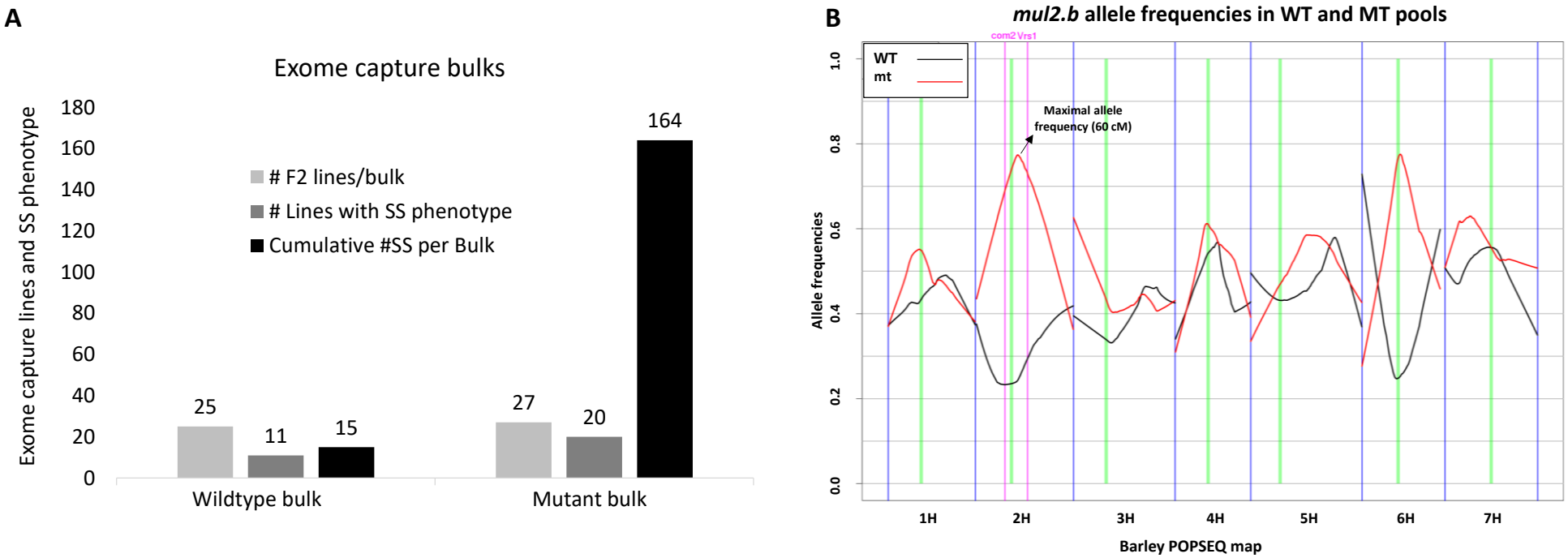
A
Exome capture bulks
Exome capture lines and SS phenotype
180
160
140
120
100
80
60
40
20
0
# F2 lines/bulk
# Lines with SS phenotype
Cumulative #SS per Bulk
25
11
15
27
20
164
Wildtype bulk
Mutant bulk
B
mul2.b allele frequencies in WT and MT pools
com2 Vrs1
WT
mt
Maximal allele frequency (60 cM)
Allele frequencies
1.0
0.8
0.6
0.4
0.2
0.0
1H
2H
3H
4H
5H
6H
7H
Barley POPSEQ map

# Figure 5

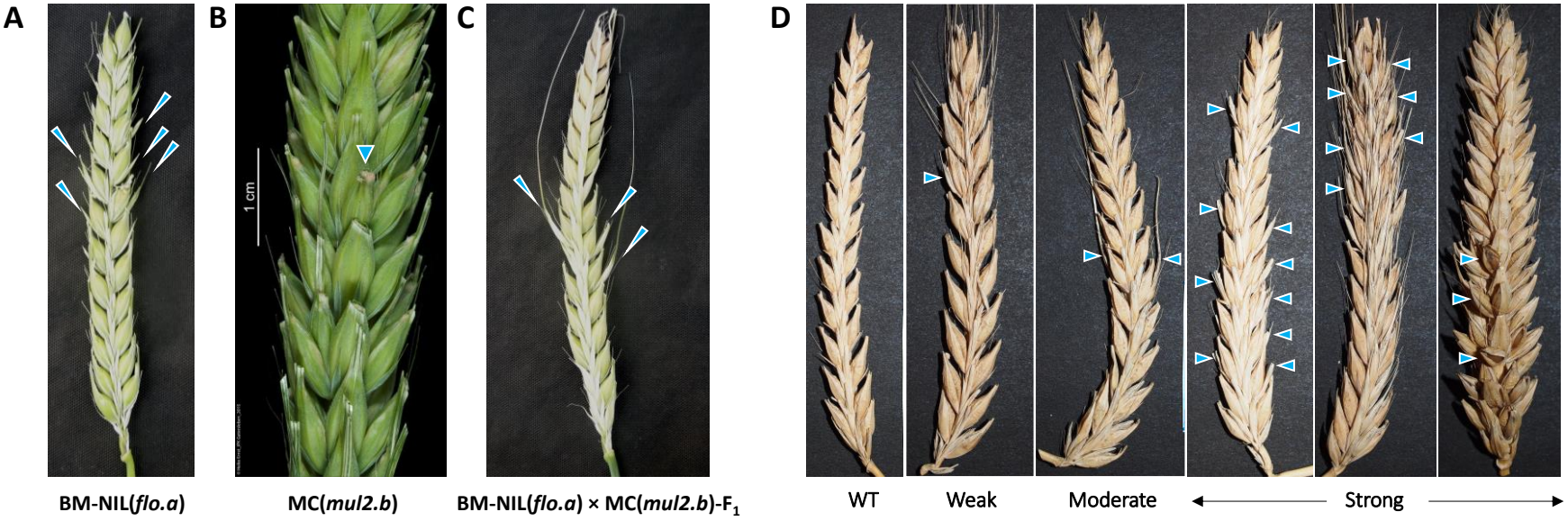


**E** BM-NIL(*flo.a*) × MC(*mul2.b*)-F$_2$ supernumerary spikelet phenotypes

| Genotype | Allele combination | Dihybrid proportion | ss recessive | SS dominant |
|---|---|---|---|---|
| FFSS | FF & SS double dominant | 1 | No | Yes |
| FFSs | FF dominant + Ss heterozygote | 2 | No | Yes |
| FfSS | Ff heterozygote + SS dominant | 2 | No | Yes |
| FfSs | Ff & Ss heterozygotes | 4 | May be | Yes |
| FFss | FF dominant + ss recessive | 1 | Yes | No |
| Ffss | Ff heterozygote + ss recessive | 2 | Yes | No |
| ffSS | ff recessive + SS dominant | 1 | Yes | Yes |
| ffSs | ff recessive + Ss heterozygote | 2 | Yes | Yes |
| ffss | ff & ss double recessive | 1 | Yes | Yes |
| Expected lines with mutant phenotype for two genes (%) | | | 68.57% | 81.04% |
| Observed lines with additional spikelet (weak to strong flo.a phenotype) | | | 73.16% | 73.16% |
| Chi-squared (1df) | | | 3.859 | 15.965 |
| P-value | | | 0.0495 | <0.0001 |

F – Dominant *FLO.A*; S – dominant second supernumerary spikelet locus; f – Recessive *flo.a*; s – recessive second supernumerary spikelet locus; S/s & F/f - Heterozygote

# Figure 6

**A**

**Morex × *mul2.b* - $F_2$ genotype, phenotype conflicts in the *mul2.b* candidate genomic interval**

| **2H markers** | l.35 | l.83 | l.84 | l.102 | l.62 | l.78 |
|---|---|---|---|---|---|---|
| M9646 - 33.7 | B | B | H | B | B | H |
| FZP-PROM3 | B | B | H | B | B | H |
| M1557975 - 50.0 | B | B | H | B | A | H |
| M1865727 - 53.3 | B | B | H | B | A | H |
| M5729 - 60.5 | B | B | B | B | A | A |
| M41820 - 61.5 | B | B | B | B | A | A |
| M47875 - 66.3 | B | B | B | B | A | A |
| M37913 - 70.8 | B | B | B | B | A | A |
| M41923 - 79.9 | B | H | B | B | A | H |
| M121208 - 87.7 | H | H | B | B | A | H |
| *mul2.b-Class I* | - | - | - | - | - | - |
| *mul2.b-Class II* | - | - | - | - | - | - |
| *mul2.b-Class III* | - | - | - | - | 2 | 3 |
| *mul2.b-Class IV* | - | - | - | - | 1 | - |
| Phenotype call | wt | wt | wt | wt | mt | mt |

A = Morex allele; B = *mul2.b* allele; H = Morex/*mul2.b*

**B**

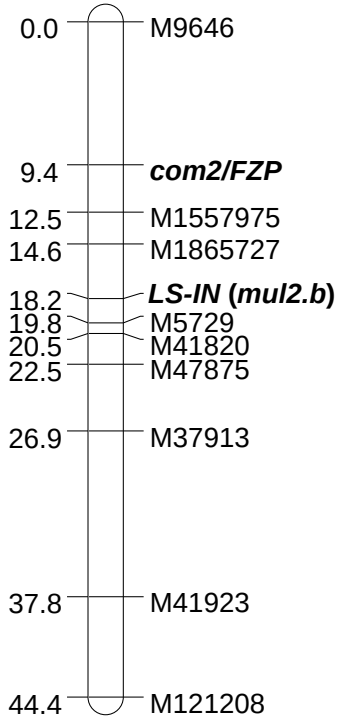


**C**

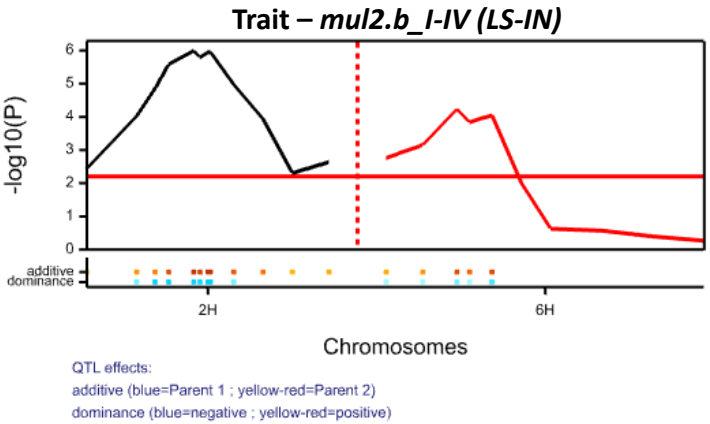


**D**

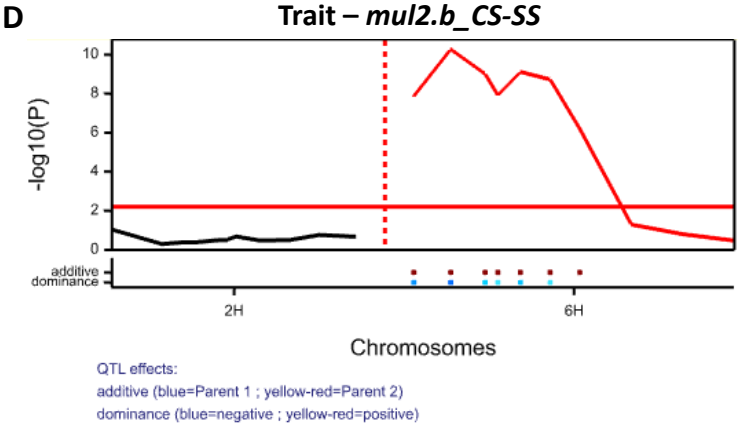


**E**

| Trait | QTL | Chr. | Position (cM) | log10(P) | %Expl. Var. | Add. eff. | High allele | Dom. eff. | Dominant allele |
|---|---|---|---|---|---|---|---|---|---|
| *mul2.b_LS-IN* | M5729 | 2H | 18.7 | 5.435 | 9.565 | 7.608 | *mul2.b* | 7.168 | Morex |
| *mul2.b_LS-IN* | FL209450 | 6H | 12.38 | 3.945 | 11.632 | 8.39 | *mul2.b* | 6.17 | Morex |
| *mul2.b_CS-SS* | FL52245 | 6H | 6.41 | 8.787 | 21.428 | 3.352 | *mul2.b* | 2.944 | Morex |

# Figure 7

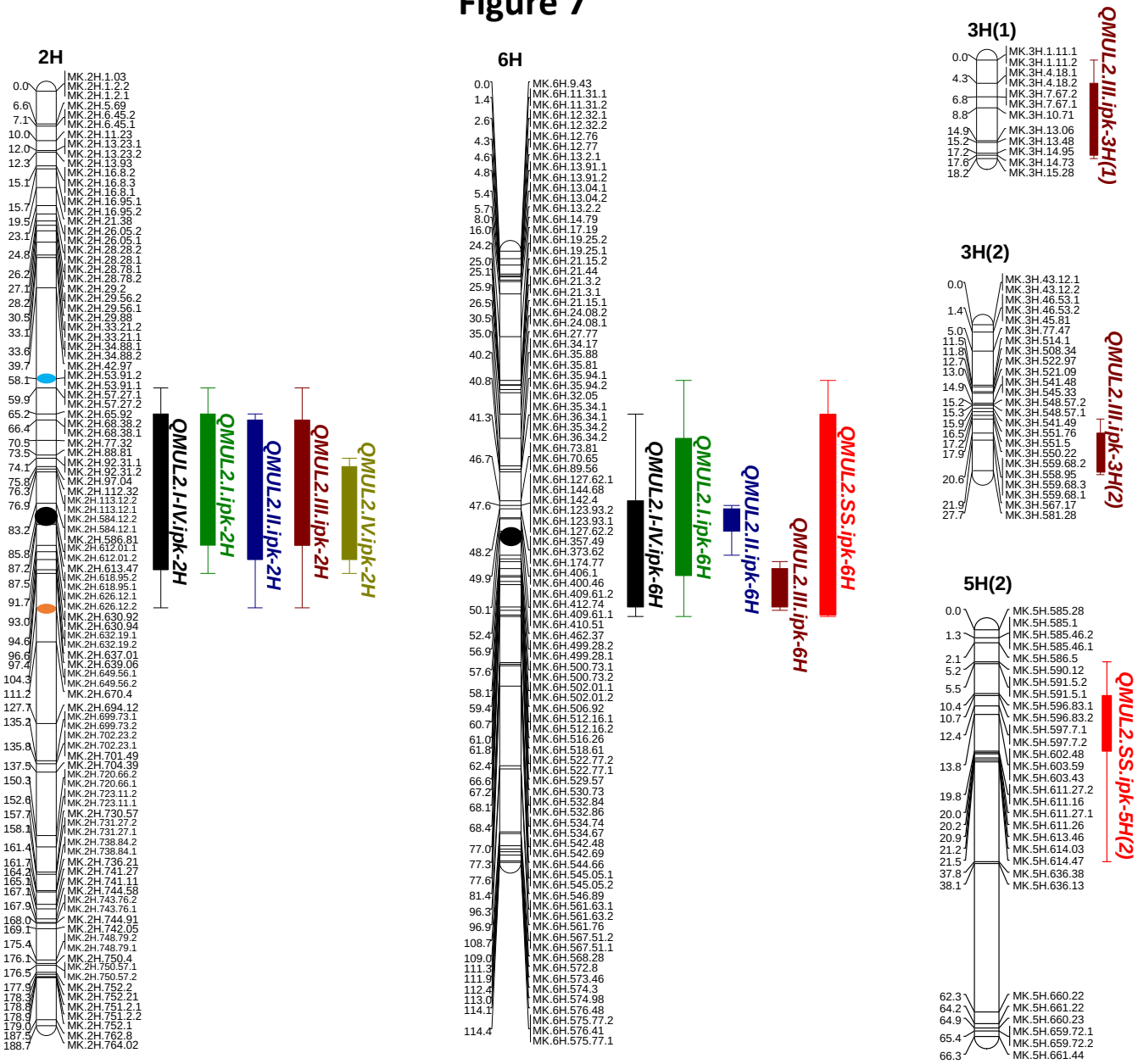


Approximate physical location of barley *COMPOSITUM 2* (*COM2*)

*SIX-ROWED SPIKE 1* (*VRS1*)

Centromere

**Supplementary figure 1**

## MYP at ~W8.0, fertile and sterile spikelets after anthesis-GH experiment 2020

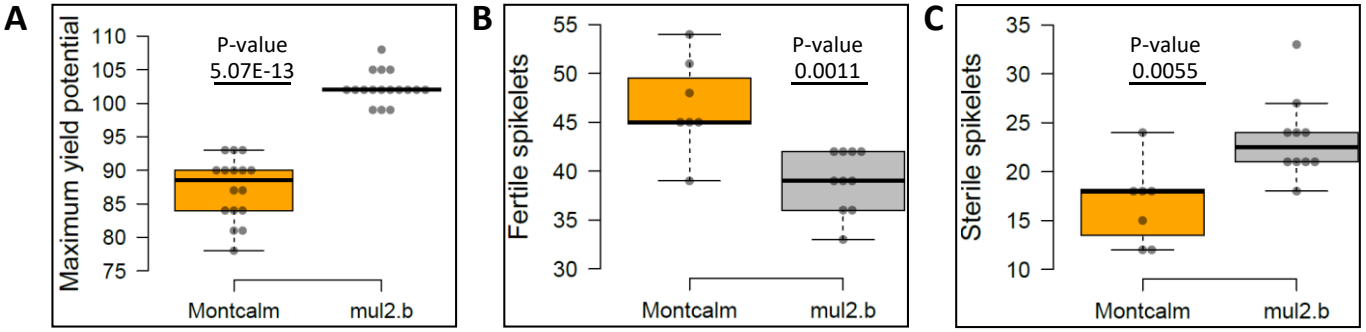


## Plant height and tillers-GH experiment 2020

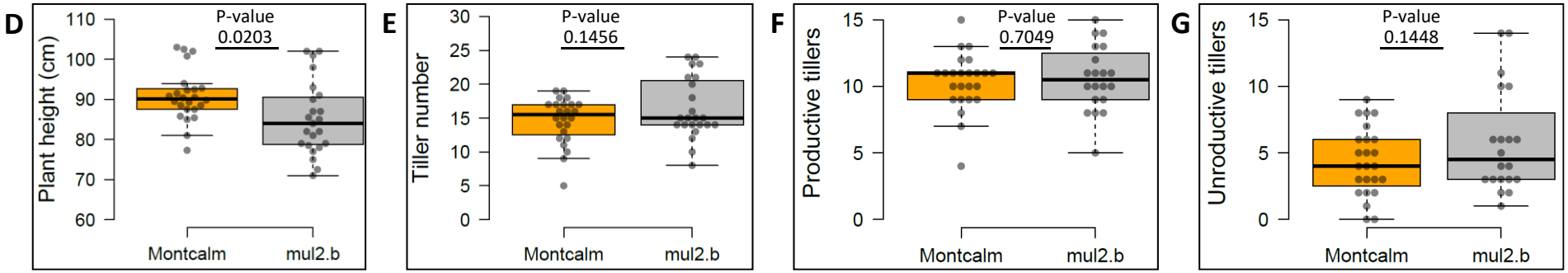

## Supplementary figure 2

### Grain morphometry parameters – central and lateral spikelet grains combined

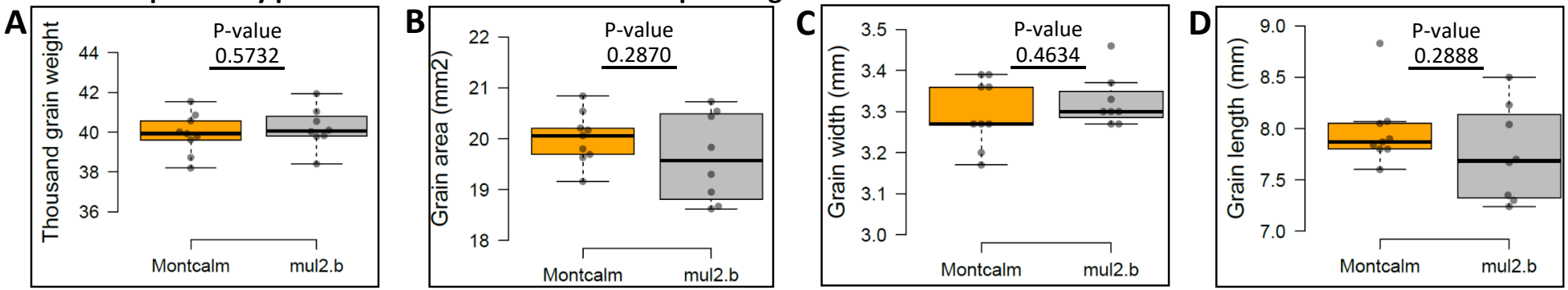


### Grain morphometry parameters – central spikelet grains

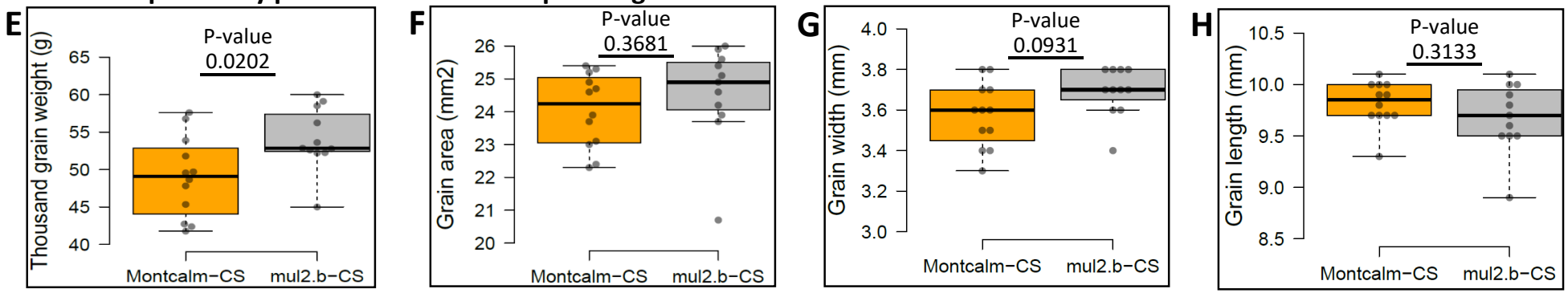


### Grain morphometry parameters – lateral spikelet grains

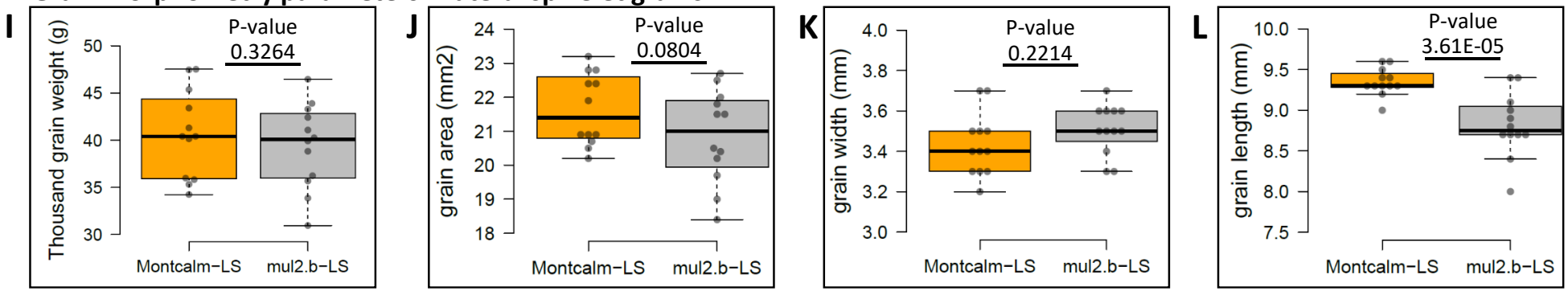

**Supplementary figure 3**

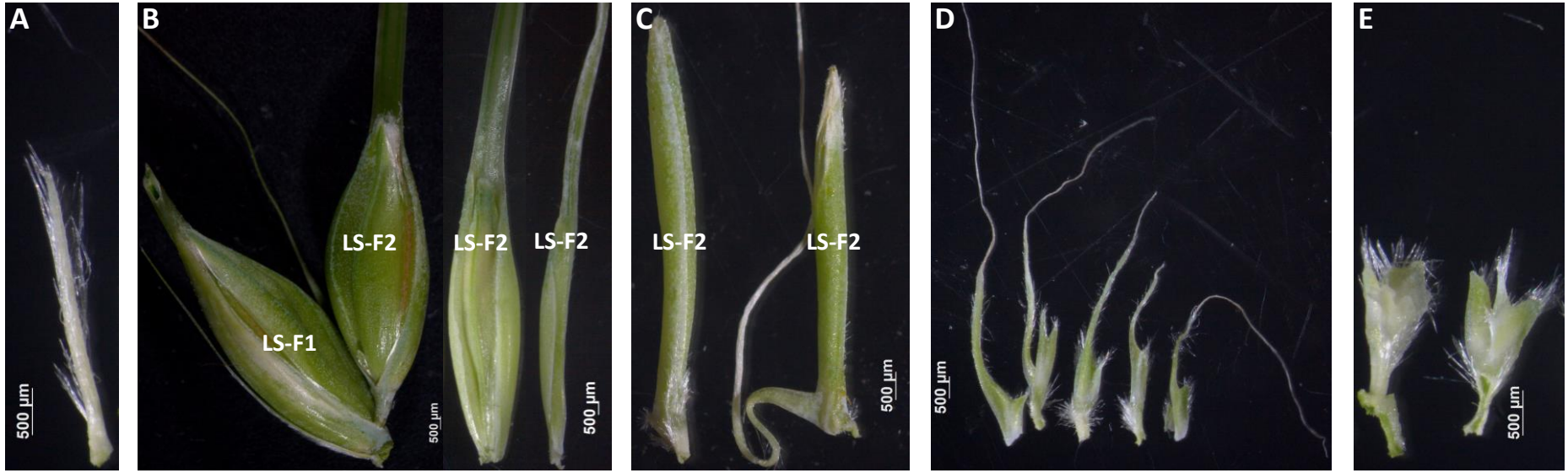


**Wt – lateral spikelet rachilla**

***mul2.b* – Class I phenotype**

***mul2.b* – Class II**

***mul2.b* – Class III**

***mul2.b* – Class IV**

## Supplementary figure 4

| | Spike 1 | | | Spike 2 | | | Spike 3 | | | Spike 4 | | | Spike 5 | | | Spike 6 | | | Spike 7 | | | Spike 8 | | | Spike 9 | | | Spike 10 | | | Spike 11 | | | Spike 12 | | |
|---|---|---|---|---|---|---|---|---|---|---|---|---|---|---|---|---|---|---|---|---|---|---|---|---|---|---|---|---|---|---|---|---|---|---|---|---|
| | LL | CS | RL | LL | CS | RL | LL | CS | RL | LL | CS | RL | LL | CS | RL | LL | CS | RL | LL | CS | RL | LL | CS | RL | LL | CS | RL | LL | CS | RL | LL | CS | RL | LL | CS | RL |
| Node 37 | ! | ! | ! | | | | | | | | | | | | | | | | | | | | | | | | | | | | | | | | | |
| Node 36 | ! | ! | ! | | | | | | | | | | | | | | | | | | | | | | ! | ! | ! | ! | ! | ! | | | | | | |
| Node 35 | ! | ! | ! | | | | | | | | | | | | | | | | | | | | | | ! | ! | ! | ! | ! | ! | | | | | | |
| Node 34 | ! | ! | ! | | | | | | | | | | | | | ! | ! | ! | ! | ! | ! | ! | ! | ! | ! | ! | ! | ! | ! | ! | ! | ! | ! | ! | ! | ! |
| Node 33 | ! | ! | ! | ! | ! | ! | ! | ! | ! | ! | ! | ! | | | | ! | ! | ! | ! | ! | ! | ! | ! | ! | ! | ! | ! | ! | ! | ! | ! | ! | ! | ! | ! | ! |
| Node 32 | ! | ! | ! | ! | ! | ! | ! | ! | ! | ! | ! | ! | ! | ! | ! | ! | ! | ! | ! | ! | ! | ! | ! | ! | ! | ! | ! | ! | ! | ! | ! | ! | ! | ! | ! | ! |
| Node 31 | ! | ! | ! | ! | ! | ! | ! | ! | ! | ! | ! | ! | ! | ! | ! | ! | ! | ! | ! | ! | ! | ! | ! | ! | ! | ! | ! | ! | ! | ! | ! | ! | ! | ! | ! | ! |
| Node 30 | ! | ! | ! | ! | ! | ! | ! | ! | ! | ! | ! | ! | ! | ! | ! | ! | ! | ! | ! | ! | ! | ! | ! | ! | ! | ! | ! | ! | ! | ! | ! | ! | ! | ! | ! | ! |
| Node 29 | ! | ! | ! | ! | ! | ! | ! | ! | ! | ! | ! | ! | ! | ! | ! | ! | ! | ! | ! | ! | ! | ! | ! | ! | ! | ! | ! | ! | ! | ! | ! | ! | ! | ! | ! | ! |
| Node 28 | ! | ! | ! | ! | ! | ! | ! | ! | ! | ! | ! | ! | ! | ! | ! | ! | ! | ! | ! | ! | ! | ! | ! | ! | ! | ! | ! | ! | ! | ! | ! | ! | ! | ! | ! | ! |
| Node 27 | ! | ! | ! | ! | ! | ! | ! | ! | ! | ! | ! | ! | ! | ! | ! | ! | ! | ! | ! | ! | ! | ! | ! | ! | ! | ! | ! | ! | ! | ! | ! | ! | ! | ! | ! | ! |
| Node 26 | ! | ! | ! | ! | ! | ! | ! | ! | ! | ! | ! | ! | ! | ! | ! | ! | ! | ! | ! | ! | ! | ! | ! | ! | ! | ! | ! | ! | ! | ! | ! | ! | ! | ! | ! | ! |
| Node 25 | - | - | II | ! | ! | ! | ! | ! | ! | ! | ! | ! | ! | ! | ! | ! | ! | ! | ! | ! | ! | ! | ! | ! | ! | ! | ! | ! | ! | ! | ! | ! | ! | ! | ! | ! |
| Node 24 | - | - | - | ! | ! | ! | ! | ! | ! | ! | ! | ! | ! | ! | ! | ! | ! | ! | ! | ! | ! | ! | ! | ! | - | - | - | - | - | - | ! | ! | ! | ! | ! | ! |
| Node 23 | - | - | - | ! | ! | ! | ! | ! | ! | ! | ! | ! | ! | ! | ! | ! | ! | ! | ! | ! | ! | ! | ! | ! | - | - | - | - | - | - | ! | ! | ! | - | - | - |
| Node 22 | - | - | II | - | - | - | ! | ! | ! | ! | ! | ! | ! | ! | ! | ! | ! | ! | ! | ! | ! | - | - | - | - | - | - | - | - | - | ! | ! | ! | - | - | - |
| Node 21 | - | - | - | - | - | - | - | - | - | ! | ! | ! | ! | ! | ! | - | - | - | - | - | - | - | - | - | - | - | - | - | - | IV | - | - | - | - | - | - |
| Node 20 | - | - | - | II | - | - | IV | - | IV | - | - | - | IV | - | - | - | - | IV | - | - | - | - | - | - | - | - | - | - | - | - | - | - | - | - | - | - |
| Node 19 | - | - | - | - | - | - | - | - | - | - | - | - | - | - | - | - | - | - | - | - | IV | IV | - | - | - | - | - | - | - | - | - | - | - | - | - | - |
| Node 18 | - | - | - | - | - | - | - | - | - | - | - | - | IV | - | IV | - | - | - | - | SS | - | - | - | - | - | - | - | I | - | I | - | - | - | - | - | - |
| Node 17 | - | - | - | - | - | - | - | - | - | - | - | - | I | - | II | - | - | - | - | - | IV | - | - | - | IV | - | III | I | - | - | I | - | I | - | - | - |
| Node 16 | - | SS | - | - | - | - | IV | - | - | - | - | - | - | - | - | - | - | - | - | - | - | I | - | IV | IV | - | - | I | - | I | IV | - | - | - | - | - |
| Node 15 | - | SS | - | - | - | - | - | - | - | - | - | - | III | - | IV | - | - | - | - | - | IV | IV | - | - | IV | - | III | - | - | - | II | - | - | - | - | - |
| Node 14 | - | - | - | - | - | - | - | - | - | - | - | - | III | - | IV | - | - | III | - | - | - | III | SS | - | - | - | III | - | - | I | - | - | IV | - | - | - |
| Node 13 | - | SS | III | - | - | - | - | - | - | - | - | - | III | - | III | - | SS | - | - | - | - | III | - | III | I | - | IV | III | - | I | - | - | - | - | - | - |
| Node 12 | - | SS | - | - | SS | - | - | - | - | - | - | - | I | - | I | - | SS | I | - | - | I | III | - | III | - | - | III | I | - | I | - | SS | III | - | - | - |
| Node 11 | I | SS | - | III | - | - | - | - | - | - | - | - | I | - | - | IV | - | - | - | - | IV | I | - | - | III | - | III | I | - | I | - | - | - | - | - | - |
| Node 10 | I | - | IV | III | - | III | - | - | - | - | - | - | I | - | IV | - | - | - | IV | - | IV | III | - | III | IV | - | IV | I | - | I | - | - | - | - | - | - |
| Node 9 | - | - | I | I | - | - | - | - | III | - | - | III | I | - | I | - | - | - | IV | - | IV | I | - | III | I | - | III | I | - | I | - | SS | - | - | - | II |
| Node 8 | I | - | - | - | - | - | - | - | III | - | - | - | I | - | I | - | - | - | IV | - | - | I | - | I | I | - | I | I | - | I | IV | - | - | - | - | - |
| Node 7 | - | - | IV | - | - | - | - | - | - | - | - | - | I | - | I | - | - | - | I | - | I | IV | - | - | I | - | I | I | - | I | I | - | I | - | - | - |
| Node 6 | III | - | IV | - | - | - | - | - | - | - | - | - | - | - | I | - | - | - | I | - | I | - | - | - | - | - | - | - | - | III | I | - | I | - | - | - |
| Node 5 | - | - | - | IV | - | I | I | - | - | - | - | - | - | - | - | - | - | - | I | - | I | - | - | - | - | - | - | - | - | - | I | - | II | - | - | II |
| Node 4 | - | - | - | I | - | - | I | - | III | I | - | - | - | - | - | - | - | - | - | - | - | - | - | - | - | - | - | - | - | - | - | - | - | I | - | - |
| Node 3 | - | - | - | - | - | - | - | - | - | - | - | - | - | - | - | I | - | I | - | - | - | I | - | I | - | - | - | - | - | I | I | - | I | - | - | - |
| Node 2 | I | I | I | I | - | - | - | - | I | - | - | - | I | - | I | - | - | - | I | - | - | - | - | - | - | - | - | I | - | I | I | - | - | - | - | - |
| Node 1 | - | - | - | - | - | - | - | - | - | - | - | - | I | - | I | - | - | - | I | - | I | I | - | I | - | - | I | - | - | - | - | - | - | - | - | - |
| Class I | 4 | | 2 | 3 | | 1 | 2 | | 1 | 1 | | 0 | 9 | | 7 | 1 | | 2 | 5 | | 5 | 6 | | 3 | 4 | | 3 | 10 | | 12 | 6 | | 4 | 1 | | 0 |
| Class II | 0 | | 1 | 1 | | 0 | 0 | | 0 | 0 | | 0 | 0 | | 1 | 0 | | 0 | 0 | | 0 | 0 | | 0 | 0 | | 0 | 0 | | 0 | 1 | | 1 | 0 | | 2 |
| Class III | 1 | | 1 | 2 | | 1 | 0 | | 3 | 0 | | 1 | 3 | | 1 | 0 | | 1 | 0 | | 0 | 4 | | 4 | 1 | | 6 | 1 | | 1 | 0 | | 1 | 0 | | 0 |
| Class IV | 0 | | 3 | 1 | | 0 | 2 | | 1 | 0 | | 0 | 2 | | 4 | 1 | | 1 | 3 | | 6 | 3 | | 1 | 4 | | 2 | 0 | | 1 | 2 | | 1 | 0 | | 0 |
| SS | | 5 | | | 1 | | | 0 | | | 0 | | | 0 | | | 2 | | | 1 | | | 1 | | | 0 | | | 0 | | | 2 | | | 0 | |

**Supplementary figure 5**

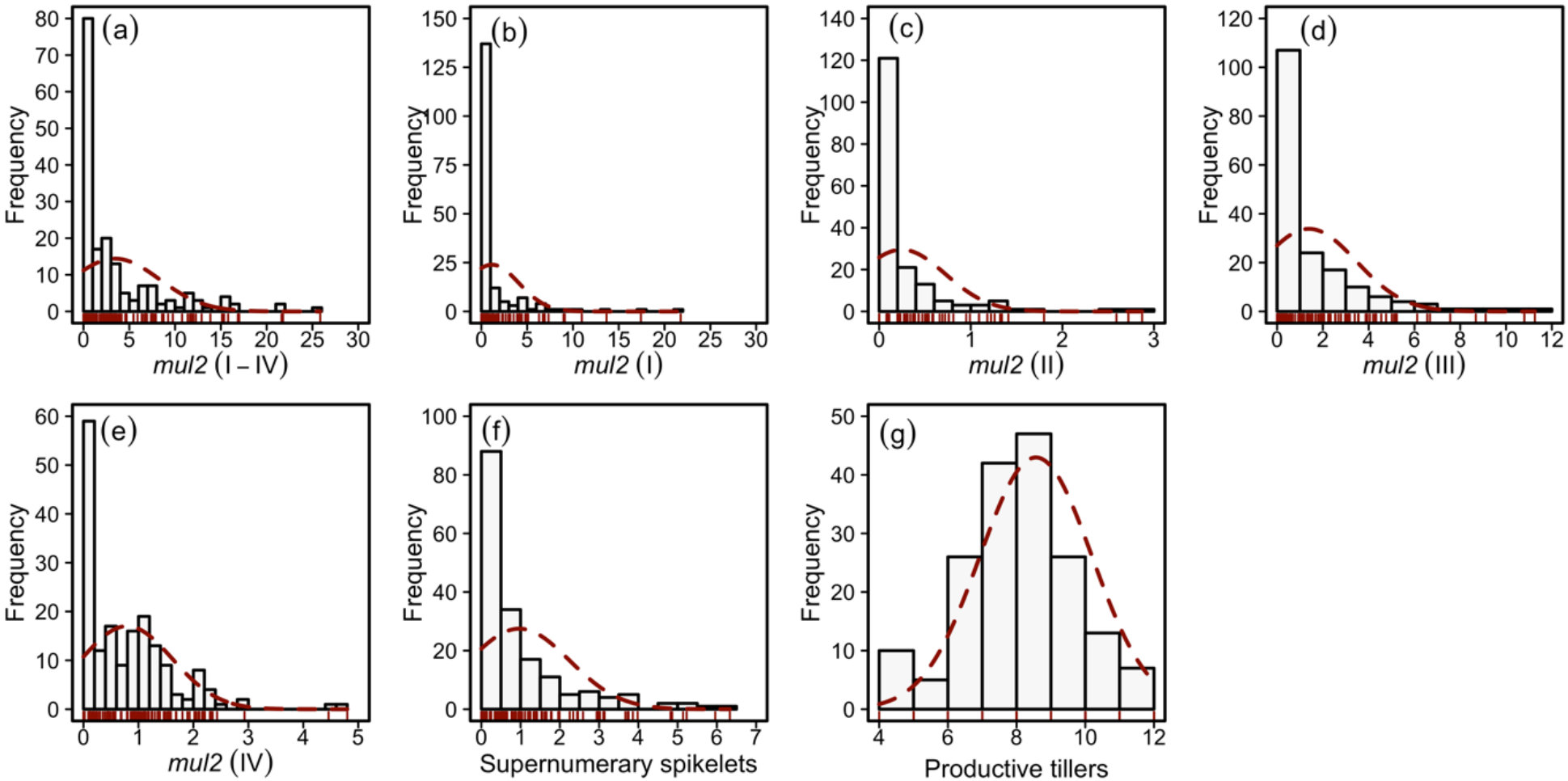

**Supplementary figure 6**

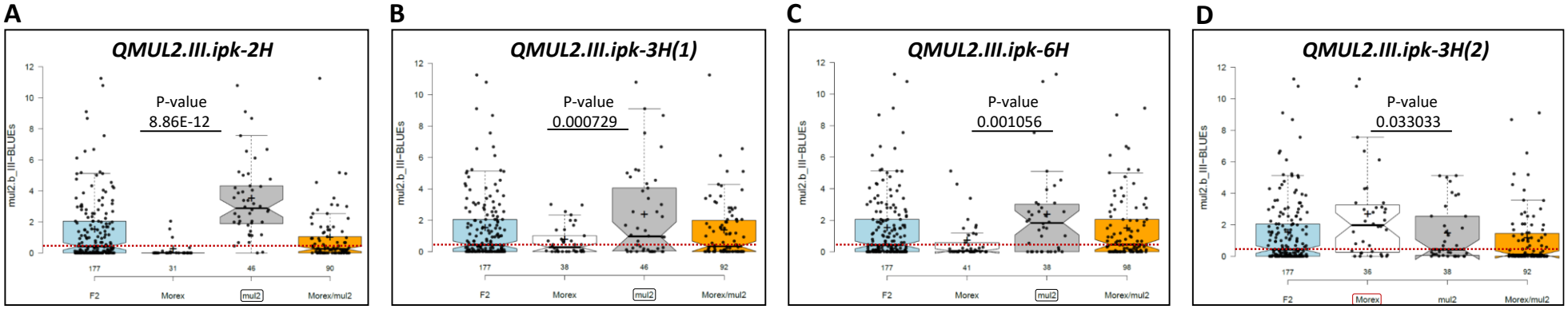


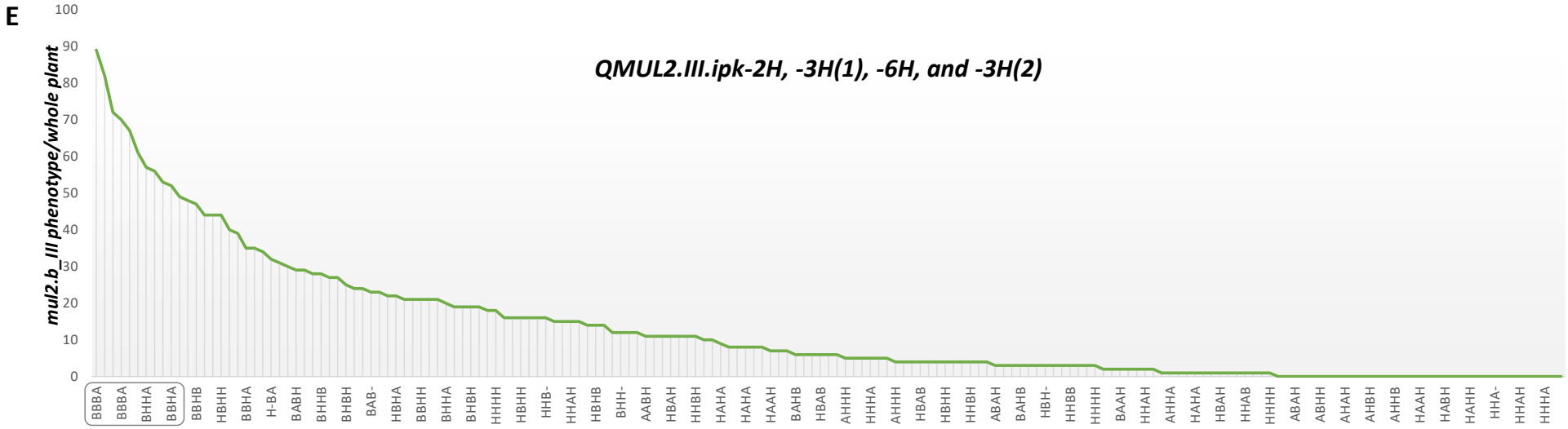


**Alleles of *mul2.b-III* 2H, 3H(1), 6H, and 3H(2) QTLS**

**Morex – A; mul2.b – B; Morex/mul2.b – H**

**Supplementary figure 7**

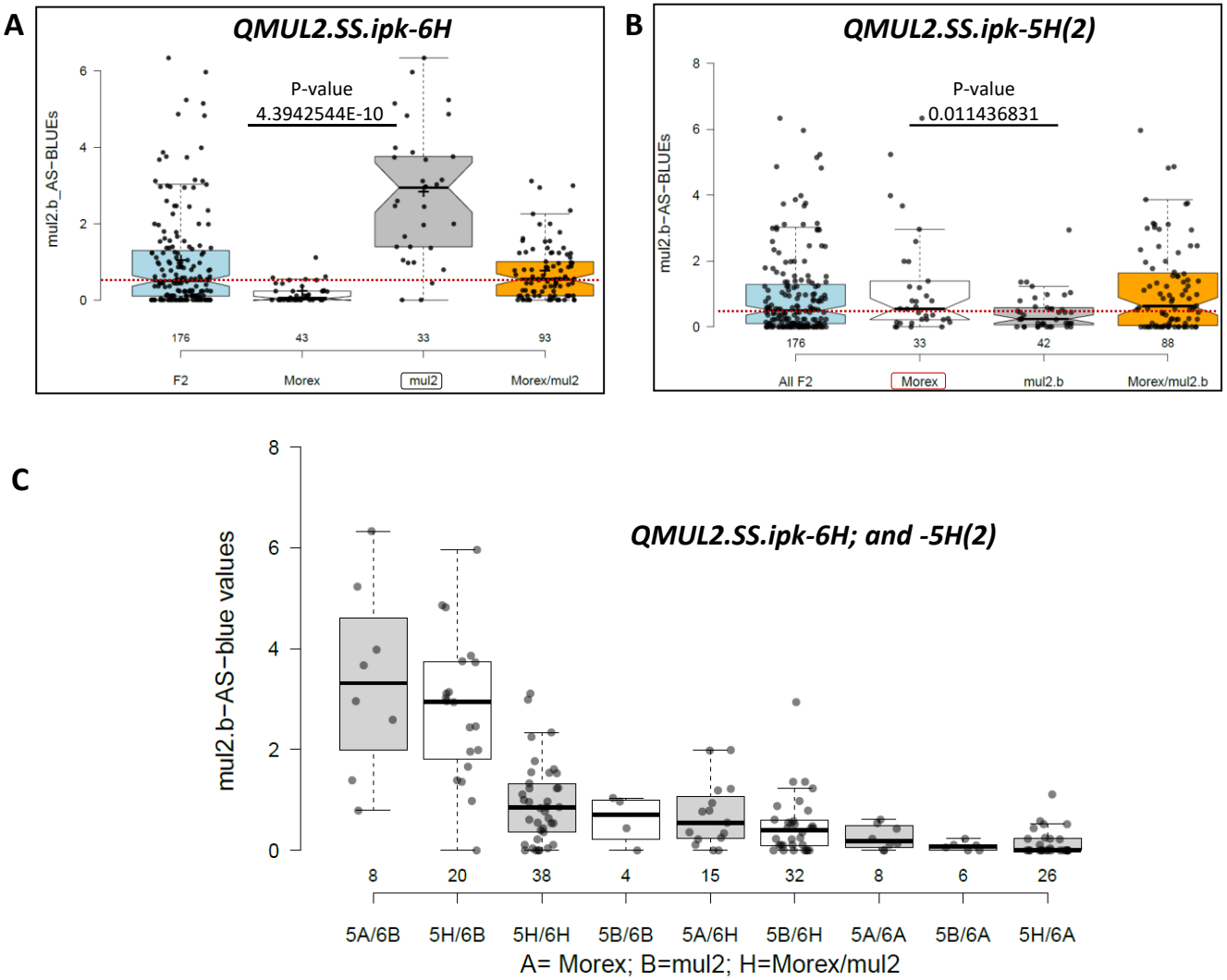

**Supplementary figure 8**

**A**

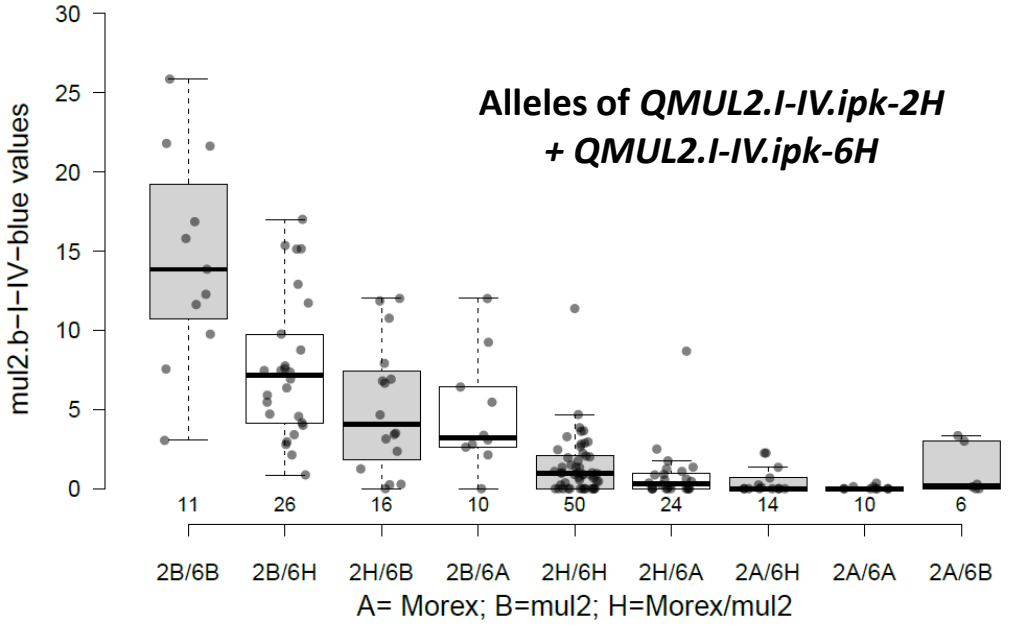


**B**

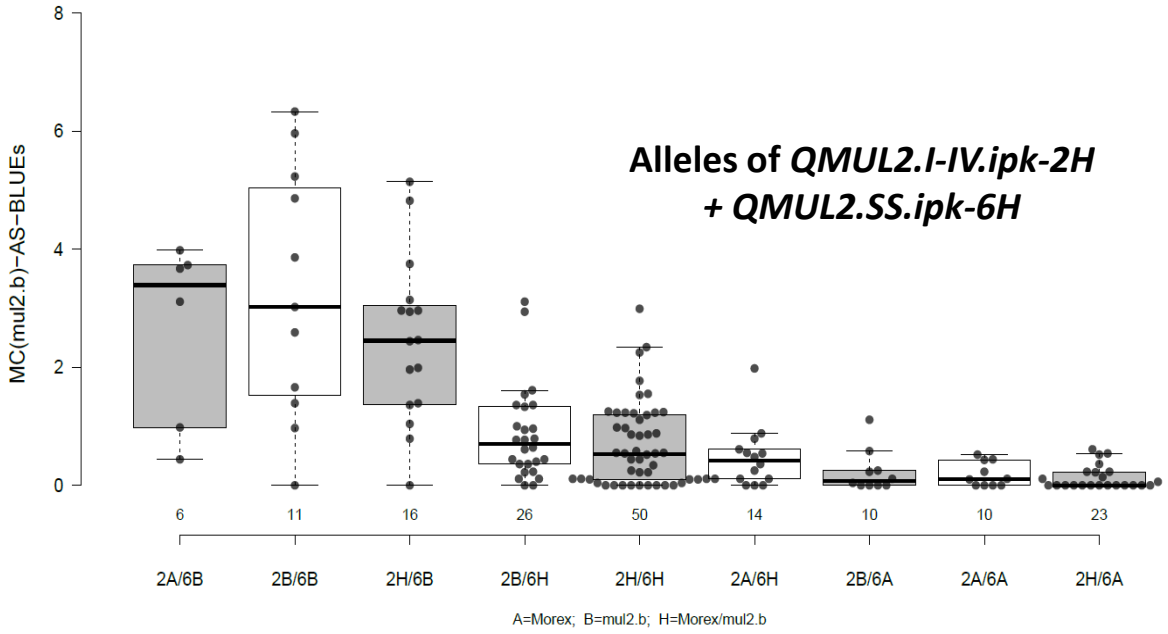

## Supplementary figure 9

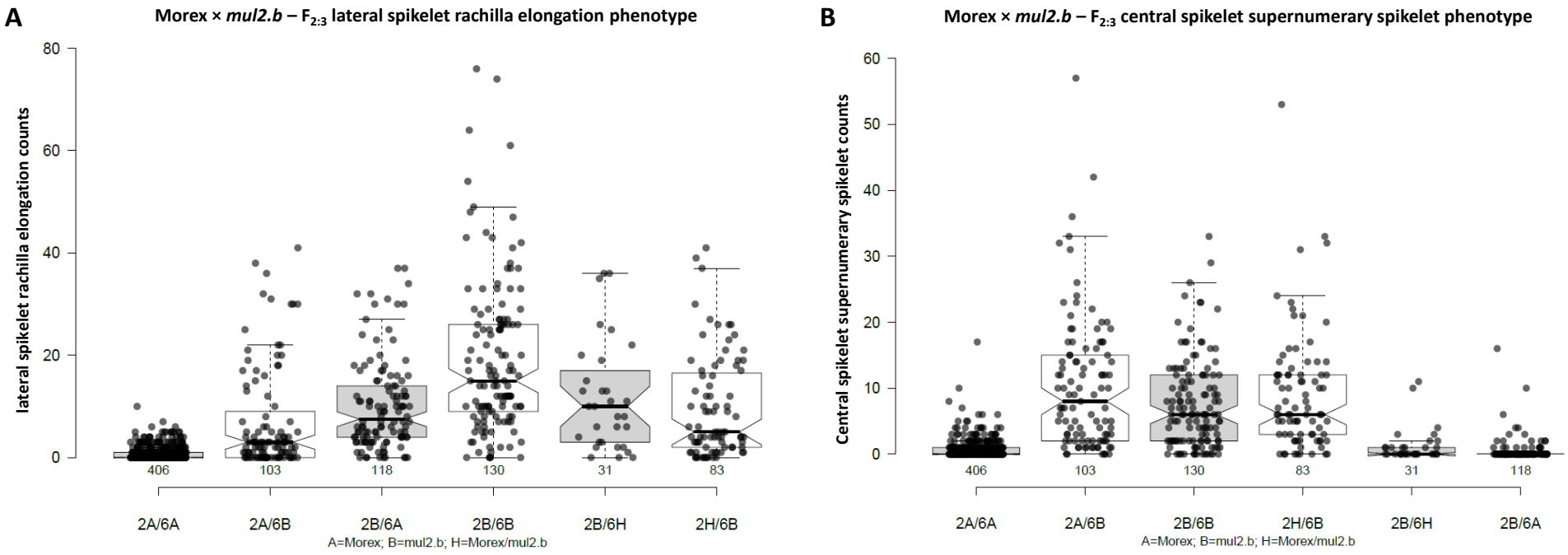

## Supplementary figure 10

BM-NIL(*mul2.b*) *mul2.b* in Montcalm